

Design, Synthesis, and Evaluation of 3,5-Disubstituted 7-Azaindoles as Trk Inhibitors with Anticancer and Antiangiogenic Activities

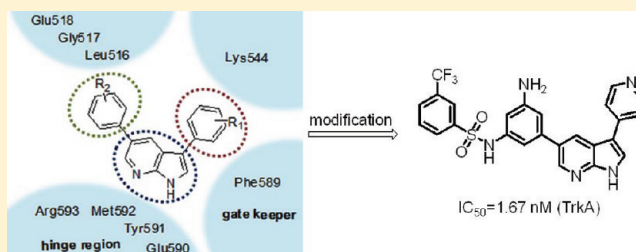
Seunghye Hong,^{†,§} Jinhee Kim,^{†,§} Ju Hyeon Seo,^{‡,§} Kyung Hee Jung,[‡] Soon-Sun Hong,^{*,‡} and Sungwoo Hong^{*,†}

[†]Department of Chemistry, Korea Advanced Institute of Science and Technology (KAIST), Daejeon 305-701, Korea

[‡]Department of Biomedical Sciences, College of Medicine, Inha University, Incheon, 400-712, Korea

S Supporting Information

ABSTRACT: Tropomyosin-related kinase A (TrkA) is considered a promising target in the development of a therapeutic treatment of cancer and pain. In this study, we designed and synthesized a series of novel 7-azaindole-based Trk kinase inhibitors through the structure-based design strategy. By varying the functional groups at the 3 and 5 positions of a 7-azaindole scaffold, we studied the structure–activity relationships (SAR) profiles and identified a series of potent Trk inhibitors. Representative derivatives showed desirable activity in cellular proliferation and apoptosis assays. Moreover, these inhibitors exhibited noteworthy antiangiogenic activity.



INTRODUCTION

Receptor tyrosine kinases (RTKs) are transmembrane receptors that phosphorylate tyrosine residues with specificity in various protein substrates. RTKs play an important role in cell signaling and are involved in a variety of normal and cancer related processes including cell migration, proliferation, survival, angiogenesis, and metastasis. The RTK family includes tropomyosin-related kinases (Trk's) that serve as receptors for neurotrophin and play a critical role in the development and maintenance of the central and peripheral nervous systems.¹ This kinase subfamily includes three homologous isoforms: TrkA, TrkB, and TrkC.² Defective TrkA signaling observed in patients of various ethnic groups has been shown to have the effect of preventing them from being able to adequately perceive painful stimuli. Besides their role in the formation and maintenance of neuronal cells, a growing body of experimental evidence has indicated that Trks are involved in malignant transformation, metastasis, survival, migration, and invasion signaling in a variety of human cancers including breast, colon, pancreatic, papillary thyroid prostate, and lung cancers and neuroblastoma.^{3–8}

In addition, recent studies have indicated that Trk compounds play important roles in angiogenesis and in the expression of HIF-1 α and VEGF.^{9,10} Angiogenesis, the formation of new blood vessels from preexisting one, is a crucial step for tumor growth, invasion, and metastasis. The transcription factor hypoxia-inducible factor 1 (HIF-1) is a major regulator of tumor cell adaptation to hypoxic stress. HIF-1 has been implicated in the up-regulation of angiogenic factors including vascular endothelial growth factor (VEGF), heme oxygenase 1, and inducible nitric oxide synthase (iNOS). Our research was stimulated by the observation that inhibition of

Trks could produce antiangiogenic activity useful against human cancers. Despite their potential as cancer therapeutic targets, only a few Trk inhibitors have been studied to explore their effect on major cancer diseases.^{11–16} Herein, we report the identification of new 7-azaindole-based Trk inhibitors that demonstrate anticancer and antiangiogenic effects in human breast cancer cells. The design strategy for improving their potency using docking simulations in ATP-binding sites to analyze the binding mode in detail was also discussed.

RESULTS AND DISCUSSION

Identification of 7-Azaindole-Based Trk Inhibitors.

The availability to control the 3D-structure of therapeutic targets has enhanced opportunities for the rapid identification of biologically active compounds utilizing structure-based drug design.^{17–19} Although the structures of the Trk extracellular ligand-binding domains have been published, the structure of the kinase domain has not yet been reported. The absence of structural information describing the nature of Trk–inhibitor interactions has made it difficult to design potent Trk inhibitors. Through a concurrent program supporting the development of PI3K inhibitors, we synthesized a set of kinase-targeted compound library based on an azaindole scaffold.²⁰ Extensive kinase cross-screening of our compound collection revealed that a 7-azaindole scaffold combined with a pyridylsulfonamide group at C5 and phenylsulfonamide group at C3 exhibited moderate activity against TrkA (POC = 9.6). To our knowledge, the 7-azaindole scaffold is not present in any of the Trk inhibitors reported so far. The newly identified

Received: March 2, 2012

Published: May 10, 2012

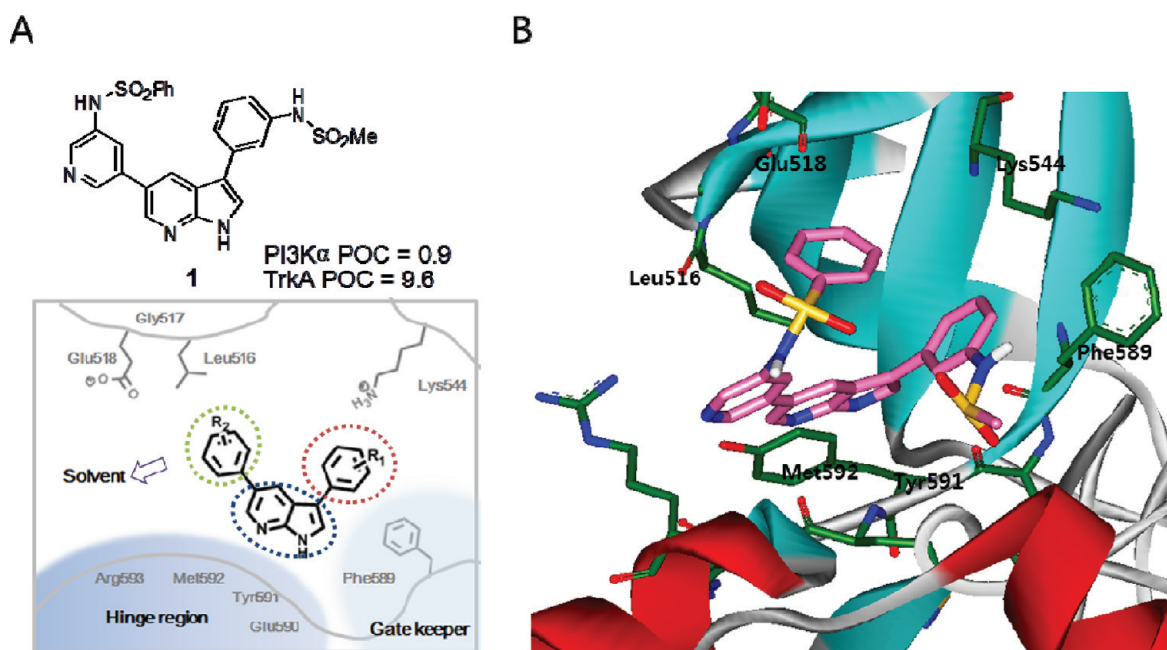


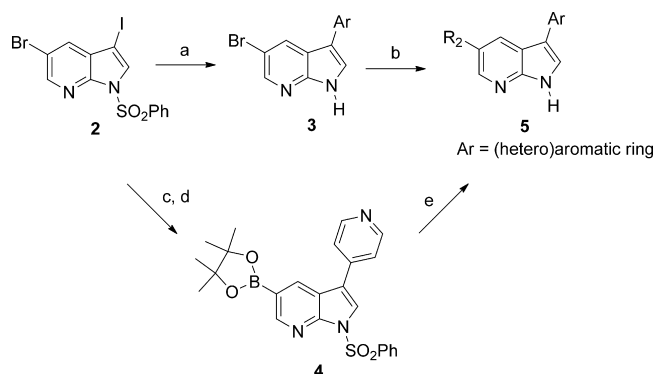
Figure 1. (A) Azaindole **1** guides the design of the Trk kinase inhibitor. (B) Calculated binding mode of compound **1** in the ATP-binding site of the TrkA homology model. Carbon atoms of compound **1** are indicated in pink.

inhibitor compound **1** may impair TrkA catalytic activity by specifically binding to the ATP binding site (Figure 1B). Considering the tolerance within the TrkA active site, compound **1** was expected to serve as a good scaffold from which more potent inhibitors could be derivatized. In addition, the series was attractive because a 7-azaindole scaffold can be easily diversified in the 3 and 5 positions via a convergent synthetic approach for the rapid elucidation of structure–activity relationship (SAR). For these reasons, compound **1** was selected for further optimization by in-depth structural modification. Structure-based mechanisms that lead to the high affinity of compound **1** to TrkA were gained through comparative investigations of the mode of binding to the ATP binding site. Figure 1B describes the lowest-energy conformation of compound **1** in the ATP binding site of TrkA, as calculated using the modified AutoDock program (see Experimental Section).²¹ The docking simulation started with the calculation of 3D grids of interaction energy for all possible atom types. These uniquely defined potential grids for TrkA were then used in common for docking simulations. For the center of the common grids, we used the center of mass coordinates of the IGF1R inhibitor²² whose binding mode in the ATP binding site of TrkA had also been predicted in the homology modeling together with the structure of TrkA itself. The calculated grid maps had dimensions of $61 \times 61 \times 61$ points with a spacing of 0.375 \AA , which yielded a receptor model that includes the atoms within 22.9 \AA of the grid center. These grid maps are actually sufficient to cope with the entire part of the kinase domain of TrkA. Hydrogen bonding groups on the 7-azaindole moiety appeared to point toward the hinge region with the hydrophobic groups situated in proximity to the amino acid residues in the ATP binding site. In addition, this structure suggested that the phenyl ring of compound **1** would be π -stacking with the Phe589 gatekeeper residue.

Improving Selectivity over PI3K. Since the initial hit **1** was found to be moderately potent against TrkA (POC = 9.6) and was more potent against PI3K α (POC = 0.9), our initial

SAR efforts were focused on improving selectivity against PI3K while maintaining potent Trk inhibition. There are structural differences in PI3K and Trk around the moiety at the 5 position of compound **1**. Therefore, we hypothesized that the proper orientation and modification of the C5 pyridyl sulfonamide group are essential for creating selective Trk inhibitors. In particular, we were interested in the one conserved water molecule that establishes the hydrogen bonding network with Tyr867, Asp841, and the ligand in ligand-bound PI3K. This ligand binding interaction plays a significant role in complex structure stabilization. In the case of compound **1**, the pyridyl nitrogen at the 5 position seemed to form hydrogen bonds with the bound water molecule in PI3K, and this interaction was not expected in Trk compounds. Our initial survey of the C5 group disturbing this key intermolecular hydrogen bond was conducted, probing the structural differences affecting the binding pockets of PI3K and Trks.

The 7-azaindole scaffold can be easily equipped with functional groups at the C5 position by standard synthetic chemistry, allowing substitutions for rapid exploration of the SAR profile. Scheme 1 illustrates the general synthetic route for the preparation of substituted azaindole derivatives. In all cases, the C3 position of the azaindole was functionalized prior to performing a Suzuki coupling with the C5 (hetero)aryl partners. Various aryl groups were attached to the 3-position of the azaindole core of **2** using palladium-mediated cross-coupling. The benzenesulfonyl group was then deprotected to yield the desired product **3**. To facilitate the exploration of an assortment of C5 functional groups, compound **3** underwent another palladium catalyzed Suzuki coupling with different boronic acid derivatives. In some cases, 3-position functionalized 5-bromoazaindole was borylated via Miyaura borylation in order to introduce various aryl groups to the 5-position. Then the borylated azaindole **4** was reacted with an aryl group under Suzuki coupling reaction conditions in order to afford the desired final compound **5**.

Scheme 1. Synthetic Route of Azaindole Derivatives^a

^aReagents and conditions: (a) arylboronic acid, Pd(dppf)Cl₂, K₂CO₃, 1,4-dioxane/H₂O = 3:1, 80 °C, 3 h, then 6 N KOH, 80 °C, 30 min; (b) arylboronic acid, Pd(dppf)Cl₂, K₂CO₃, 1,4-dioxane/H₂O = 3:1, 100 °C, 5 h; (c) 4-pyridinylboronic acid, Pd(dppf)Cl₂, K₂CO₃, 1,4-dioxane/H₂O = 3:1, 80 °C, 3 h (d) bis(pinacolato)diboron, Pd(dppf)Cl₂, KOAc, 1,4-dioxane, 100 °C, 12 h; (e) aryl bromide, Pd(dppf)Cl₂, K₂CO₃, 1,4-dioxane/H₂O = 3:1, 100 °C, 5 h, then 6 N KOH, 80 °C, 30 min.

The resulting compounds were tested over PI3K α and TrkA at 10 μ M in a high-throughput binding assay (KINOMEScan, Ambit Biosciences). Of particular significance was the observation that the binding affinity over PI3K α was dramatically reduced (**5b**: POC = 31, K_d = 2300 nM for PI3K α) (Table 1) when the pyridyl group at the C5 position was replaced with a phenyl group, probably because of disruption of the key intermolecular hydrogen bond with a bound water molecule in PI3K. Interestingly, this replacement resulted in a slightly increased potency against TrkA. The sulfonyl group was not required for producing the Trk inhibitory activity. We also examined the significance of the anilinic group at C5 and observed that the binding affinity was reduced when the 3-amino group was replaced with a CN group (**5e**). Next, in order to determine whether or not the 3,4-dimethoxy phenyl group at the C3 was optimal, the effects of its replacement with other groups were explored. Of these, the 4-pyridyl group was found to be the most effective moiety in the C3 position (**5f**: POC = 0, K_d = 64 nM for TrkA) while retaining excellent selectivity over PI3K α (POC = 31, K_d = 2900 nM). The 4-pyridyl group seemed to π -stack efficiently with the Phe589, and 4-nitrogen may be an essential hydrogen bonding donor for Lys544. Considering its simple structure and low molecular weight (<300), **5f** was expected to serve as a good inhibitor scaffold from which more potent inhibitors could be derivatized. Interestingly, replacement of the 7-azaindole scaffold with the indole scaffold resulted in a complete loss of activity (POC = 72), thus revealing the indispensable nature of the 7-azaindole scaffold in maintaining activity in this series. On the basis of these findings, lead **5f** was selected for further structural modification to investigate SAR in order to optimize both the kinase and cell-based activity.

Lead Optimization. On the basis of the structure of compound **5f**, the enhanced potency of the 4-pyridyl moiety at C3 and the 3-aniline at position C5 suggested a need to more broadly explore analogues incorporating these key functional groups. Thus, we fixed a 4-pyridyl group at the C3 position of 7-azaindole and then screened various groups at the C5 position, expecting to find improved enzyme interaction and physicochemical properties. On the basis of the docking model

data, the 3-aminophenyl group at the azaindole C5 faced into the solvent front, and there was available space for amino acid residues utilizing an additional inhibitor design. We expanded the structure–activity relationship of a diverse set of substituents while aiming to modify the 3-aniline at C5 in the new analogues (Table 2). The lead **5f** was tolerant to substitution with methyl, dimethyl, or acyl group at the aniline amino group. The orientation of the amino group was not critical, as **5f** and **6f** were found to be nearly equipotent. The next round of analogues incorporated an additional substituent into the 3-aniline ring in order to identify the most suitable moiety. In this series of analogues, it appeared that the substitution around the 3-aniline ring was relatively important to its function. In general, having a substituent at the 4 or 5 position of aniline enhanced its potency, whereas a substitution at the 6 position was detrimental to Trk inhibitory activity. The substituent at the 4 position of the aniline ring was varied to include methyl, methoxy, and chloro groups, and these derivatives were all tolerated (**6g**, **6h**, **6i**). The morpholine moiety was employed to enhance the physicochemical properties, but replacement of the methoxy group with morpholinomethanone (**6j**) affected a slightly decreased potency. This trend was similar to the one found for the substituent at the 5 position of the aniline ring when comparing compounds **6l** and **6m**. We further attempted to explore the SAR in the side chain linked to the C5 position of the aniline ring. Introducing an oxyethaneamine group into the C5 position of the aniline yielded an increase in Trk inhibitory activity (**6n** and **6o**). In this series, benzenesulfonamide substitution of the aniline also provided a boost in potency (**6q** IC₅₀ = 9.4 nM). This prompted us to further investigate the effect of various sulfonyl groups on Trk binding affinity. Notably, *m*-CF₃-containing analogue **6t** was an exceptionally potent Trk inhibitor with an IC₅₀ of 1.67 nM. Next, we attempted to replace the sulfonamide group with amide (**6u**), which also showed nanomolar level inhibition. However, the amide analogue **6u** was almost inactive in the cell-based assay, which may be attributed to poor cellular permeability and water solubility. Separately, while a substitution at the 4- or 5-position of the 3-aniline ring was relatively well tolerated, a substitution at the 6-position was deleterious to inhibitory activity (**6v**, **6w**). Especially, when the 5-sulfonamide group was moved to the 6-position, it resulted in a drastic loss of activity (**6w**). This result demonstrated that the orientation of the 5-substituent in the aniline ring plays an important role in determining activity. With the impressive Trk enzyme activity profile, cell potency of these TrkA inhibitors was further determined in a more cancer-related setting. For this purpose, compounds from this series were tested for cellular proliferation activity against MCF-7 human breast cancer cells. To measure the inhibitory effect of compounds on cell growth, cell viability was tested by 3-(4,5-dimethylthiazol-2-yl)-2,5-diphenyltetrazolium bromide (MTT) assay in MCF-7 human breast cancer cell cultures as shown in Table 2.

Binding Mode. On the basis of the docking results and SAR, we identified the binding mode and the detailed interactions responsible for stabilizing compound **6t** in the TrkA homology model. Figure 2 shows the lowest-energy conformations of **6t** in the TrkA ATP binding site, calculated using the modified AutoDock program. The results of the docking simulations were self-consistent in the sense that compounds **1** and **6t** were positioned in similar configurations with comparable interactions with the amino acid residues in

Table 1. Azaindoles Scaffold as Trk Inhibitors

5

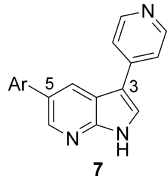
Compd	R ₁	R ₂	TrkA		PI3K α		Selectivity (over PI3K α)
			POC(%) ^a	K _d (nM)	POC(%) ^a	K _d (nM)	
5a			0.8	145	0.05	48	0.33
5b			0.2	91	31	2300	25
5c			0.05	58	12	960	17
5d			1.3	125	59	ND	-
5e			26	ND	69	ND	-
5f			0	16	31	2900	181
5g			0.2	75	42	4500	60
5h			0.3	88	100	ND	-
5i			2.6	270	98	ND	-
5j			0.65	110	48	12000	109

^aCompounds were tested against TrkA and PI3K α at 10 μ M. Lower numbers of POC (percent of control) indicate stronger hits. Values show an average of duplicate measurements.

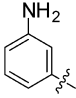
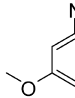
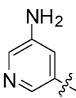
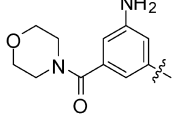
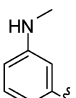
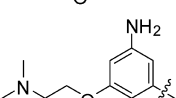
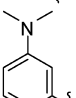
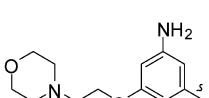
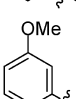
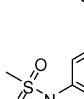
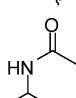
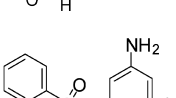
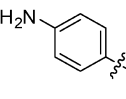
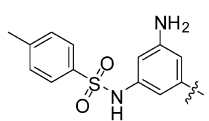
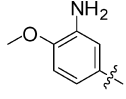
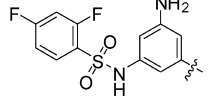
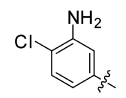
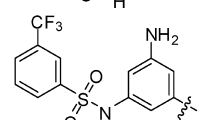
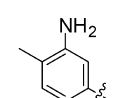
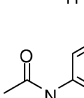
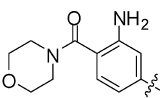
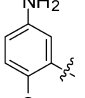
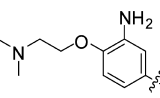
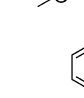
the ATP binding site. Hydrogen bonding groups on the inhibitors appeared to point toward the backbone groups of the ATP binding site, with their hydrophobic groups situated in proximity to the Gly loop. However, **6t** is more closely directed toward the pocket around Lys544 and Phe589, while compound **1** may not reach this region because of unfavorable steric interactions of the bulky sulfonamide group on the C3 phenyl ring. Therefore, nitrogen at the 4-position of the pyridyl group of **6t** can form a hydrogen bond with Lys544, and the NH group of the 7-azaindoles donates a hydrogen bond to the backbone aminocarbonyl oxygen of Glu590. In addition, the nitrogen at the 7-position of the azaindoles scaffold appeared to

form a hydrogen bond with the backbone aminocarbonyl nitrogen of Met592. The terminal anilinic group of **6t** donated a hydrogen bond to the backbone aminocarbonyl oxygen of Arg593. The sulfonamide group appeared to form a hydrogen bond with the backbone aminocarbonyl oxygen of Leu516. These five hydrogen bonds appeared to be the most significant binding forces stabilizing **6t** in the ATP binding site. Compound **6t** could be further stabilized in the TrkA ATP binding site via π -stacking interaction with the Phe589 gatekeeper residue, and hydrophobic interactions with the side chains of Met592, Phe589, Lys544, Tyr591, Gly595, Met671, Asp596, L657, and Ile675. The overall structural

Table 2. Exploration of the Groups at C5



7

Compd	Ar	TrkA IC ₅₀ (nM)	MCF-7 Growth IC ₅₀ (μM)	Compd	Ar	TrkA IC ₅₀ (nM)	MCF-7 Growth IC ₅₀ (μM)
5f		42.7	2.3	6l		18.6	8.5
6a		69.6	5.1	6m		64.7	>30
6b		31.4	4.5	6n		13.63	11.2
6c		26.47	12.1	6o		8.36	11.2
6d		22.7	11.7	6p		33.75	>30
6e		34.3	9.1	6q		9.4	8.8
6f		25.02	7.7	6r		4.62	10.4
6g		33.2	8.7	6s		2.97	6.6
6h		53.7	12.0	6t		1.67	4.2
6i		22.2	2.8	6u		5.41	>30
6j		88.6	8.5	6v		110.3	5.4
6k		47.0	3.1	6w		3167	-

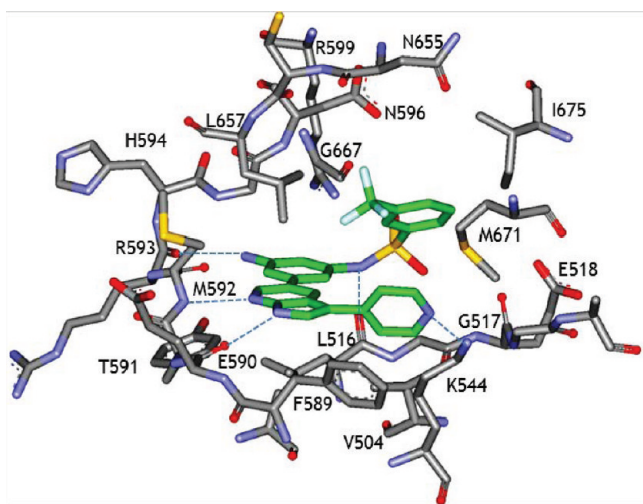


Figure 2. Calculated binding mode of **6t** in the ATP-binding site of Trk. Carbon atoms of the protein and the ligand are indicated in gray and green, respectively. Each dotted line indicates a hydrogen bond.

features derived from the docking simulations suggested that the nanomolar inhibitory activity of **6t** could be attributed to the establishment of multiple hydrogen bonds and hydrophobic interactions in a simultaneous fashion in the TrkA ATP binding site.

The most potent inhibitor **6t** was subjected to kinase selectivity profiling over a panel of 30 cancer related kinases at 1 μM in a high-throughput binding assay (KINOMEScan, Ambit Biosciences). Three kinases KIT, TrkA, and TrkB displayed tight binding to **6t** (kinases with POC < 10) as shown in Table 3. Subsequently the measured IC_{50} demonstrated that **6t** is about 100-fold selective for TrkA over KIT (TrkA IC_{50} = 1.67 nM and KIT IC_{50} = 145 nM).

Table 3. KINOMEScan Profile of Compound **6t**^a

kinase	POC ^b	kinase	POC ^b	kinase	POC ^b
ABL1	81	FGFR2	61	PDPK1	90
AKT1	94	GSK3b	81	PKAC-a	88
AKT2	100	JAK2	34	PLK1	100
AURKA	100	KIT	3	PI3KCA	64
AURKB	85	MEK1	100	PIM1	97
BRAF	100	MEK2	100	PLK1	100
CDK11	26	MET	96	PLK3	75
EGFR	100	P38 α	100	ROCK2	50
ERK1	100	PAK1	79	TRKA	0.8
FAK	88	PDGFRA	69	TRKB	1.2

^aPanel of 30 kinases were tested at 1 μM in a high-throughput binding assay (Ambit Bioscience). ^bLower numbers of POC (percent of control) indicate stronger hits. Values show an average of duplicate measurements.

MECHANISM STUDIES

The Trk pathway plays a critical role in cell progression by promoting cell proliferation and inhibiting apoptosis. For a selected Trk inhibitor, **6t** displaying both potent enzymatic and cellular activity and the mechanism of cancer cell death was assessed, followed by an antiangiogenic evaluation.

Effect on Cell Proliferation and Cell Signaling Downstream. In order to identify the anticancer effect of **6t**, we

compared the cell growth in three human breast cell lines (MDA231, MCF-7, and SKBr3) after treatment by **6t** using a 3-(4,5-dimethylthiazol-2-yl)-2,5-diphenyltetrazolium bromide (MTT) assay. We observed that **6t** clearly induced cell death in MCF-7 and SKBr3 human breast cancer cells in a dose-dependent manner (Figure 3A). In particular, **6t** induced strong cell growth reduction in MCF-7 human breast cancer cells in a range between 40% and 70%. Trk pathway stimulates the PI3K/Akt pathway, resulting in a cascade of downstream signaling events.²³ Since the activation of the Trk pathway leads to phosphorylation of Akt, we investigated the effects of **6t** on the Trk/Akt pathway in MCF-7 human breast cancer cells. When MCF-7 human cancer cells were treated with various concentrations of **6t**, phosphorylations of TrkA and Akt were effectively suppressed (Figure 3B). The most potent compound, **6t** in enzyme assay, was moderately active in cell-based assay and Western blotting, which may be attributed to poor cellular permeability and water solubility.

Effect on Apoptotic Cell Death. The occurrence of apoptotic nuclei condensation and TUNEL reaction were investigated to determine whether or not MCF-7 cell death was a result of apoptosis. In order to characterize the cell death induced by **6t**, we examined the nuclear morphology of dying cells with a fluorescent DNA-binding agent, DAPI. MCF-7 cells treated with **6t** displayed the typical morphological features of apoptotic cells including condensed and fragmented nuclei, while homogeneous nuclear chromatin was evident in the control cells. The induction of apoptosis by **6t** was confirmed using the TUNEL assay (Figure 4A). The TUNEL assay, based on the labeling of DNA strand breaks generated during apoptosis, revealed that **6t** induced apoptosis in MCF-7 cells. In order to further explore the mechanisms of this induced apoptosis, we examined the expression of apoptotic regulatory proteins such as cytochrome C, Bcl-2, Bax and cleaved caspase-3 using immunofluorescence staining.²⁴ As expected, **6t** increased the expression of cytochrome C, Bax, cleaved caspase-3, as well as decreased the expression of Bcl-2 in MCF-7 breast cancer cells (Figure 4B). These results showed that **6t** induces cell apoptosis in MCF-7 breast cancer cells.

Effect on the Expression of HIF-1 α and VEGF. HIF-1 α is an important target modulator of angiogenic factors along with VEGF, an immediate downstream target gene of HIF-1 α . Thus, it was appropriate to investigate the effect of **6t** on the expression of hypoxia-induced HIF-1 α and VEGF. MCF-7 cells were treated with various concentrations of **6t** under hypoxia in order to mimic the conditions induced by 100 μM CoCl₂ for 6 h. As shown in Figure 5, HIF-1 α expression increased under hypoxic conditions, whereas **6t** inhibited the hypoxia-induced HIF-1 α expression in a dose-dependent manner. In addition, we identified the effects of **6t** (0.1–10 μM) on the production of the hypoxia-induced VEGF. When the cells were treated with **6t** under hypoxic conditions, the VEGF protein level reduced dramatically.

Effect on Cell Migration. The antiangiogenic activity of **6t** was further evaluated using assays including wound induced migration of human umbilical vein endothelial cells (HUVEC). Since cell migration is the one of the major processes for endothelial cells in the formation of blood vessels during angiogenesis and metastasis, we examined the effects of **6t** on the migration of HUVECs. Endothelial cells were wounded and then incubated in the presence of **6t** (1–10 μM) for 16 h. As shown in Figure 6, compound **6t** reduced the migration of HUVECs in a dose-dependent manner.

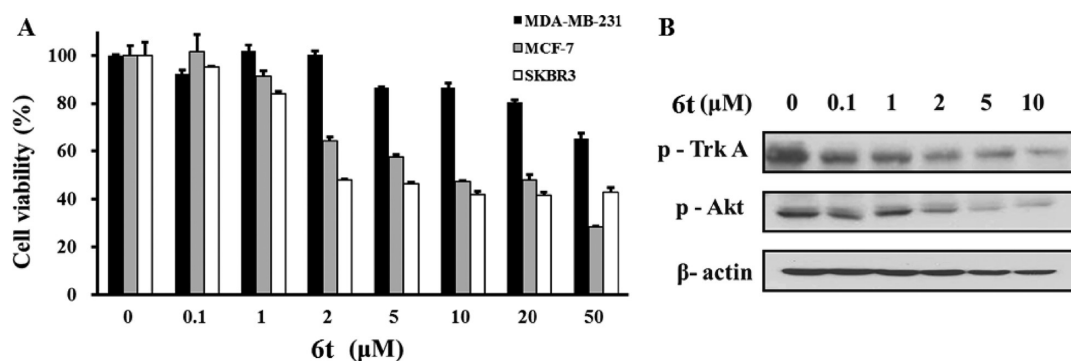


Figure 3. Effect of **6t** on the cell growth/proliferation and cell signaling pathways in human breast cancer cells. Effect of **6t** on growth/proliferation was measured in human breast cancer cells (MDA231, MCF-7, and SKBr3) by MTT assay (A). Results are expressed as a percent of relative cell proliferation compared to control. The inhibition of Trk/Akt signaling pathway by **6t** in MCF-7 cells was analyzed by Western blotting (p-Trk and p-Akt). Data are represented as the mean \pm SD from the triplicate wells (B).

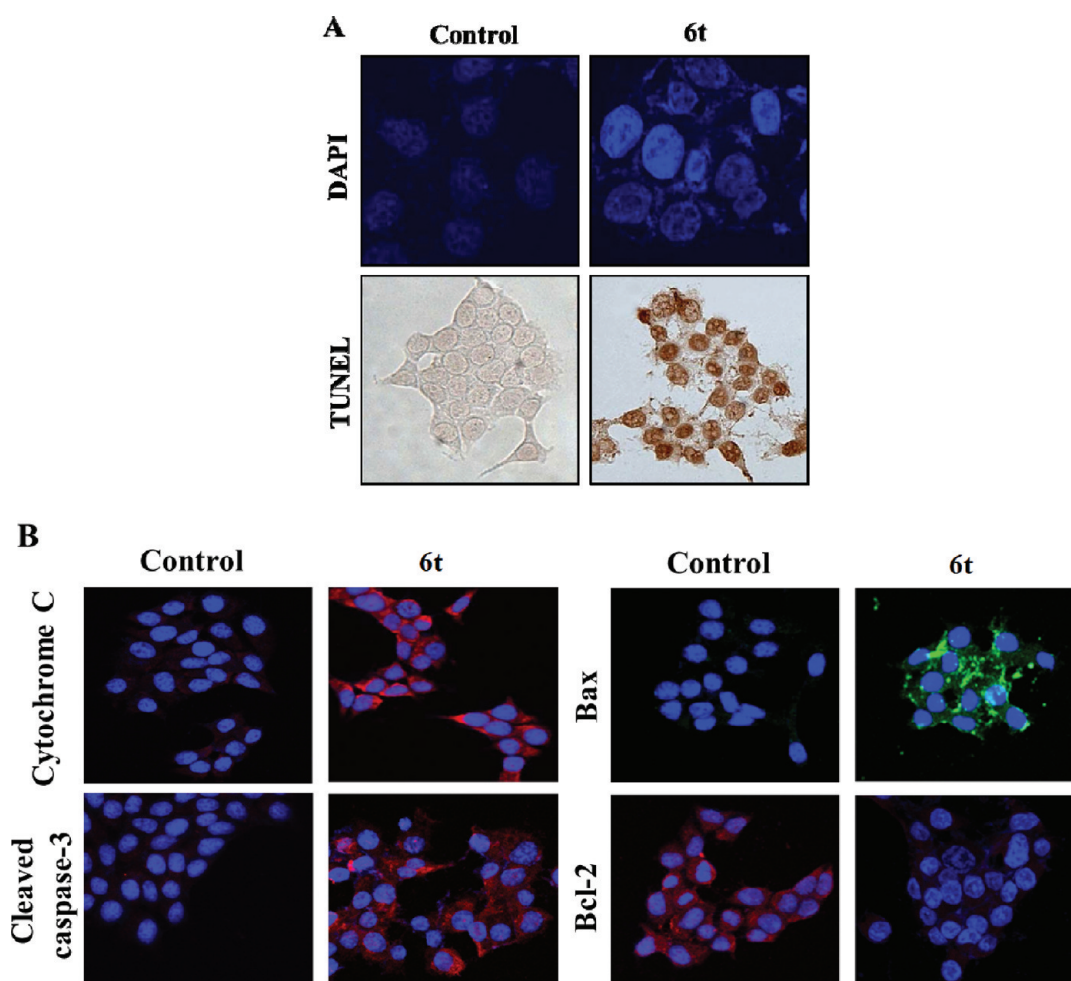


Figure 4. Effect of **6t** on the apoptosis of MCF-7 breast cancer cells. (A) MCF-7 breast cancer cells treated with **6t** ($10 \mu\text{M}$) for 24 h. The induction of apoptosis by **6t** was conducted by DAPI and TUNEL staining and photographed at $\times 400$ magnification. (B) The expressions of cytochrome C, Bcl-2, Bax, and cleaved caspase-3 were observed by immunofluorescence staining in cells treated with **6t** ($10 \mu\text{M}$) for 24 h at $\times 800$ magnification.

Effect on Tubular Network Formation. The antiangiogenic effect on tube formation was analyzed by treating HUVEC with compound **6t**. HUVECs were plated on Matrigel in order to mimic in vivo HUVEC associated angiogenesis and then treated with various concentrations of **6t** (1 – $10 \mu\text{M}$). While the HUVECs were plated, they aligned with one another and formed tubes resembling a capillary plexus. The **6t** produced significant inhibition of the VEGF-induced formation

of vessel-like structures, resulting in the elongation and alignment of the HUVECs in a dose-dependent manner (Figure 7). Considering that endothelial migration and tube formation are all highly relevant properties in the process of angiogenesis, these results showed that TrkA inhibitor **6t** has the ability to block VEGF-induced angiogenesis by suppressing hypoxia-induced VEGF expression and preventing tube formation and endothelial cell migration.

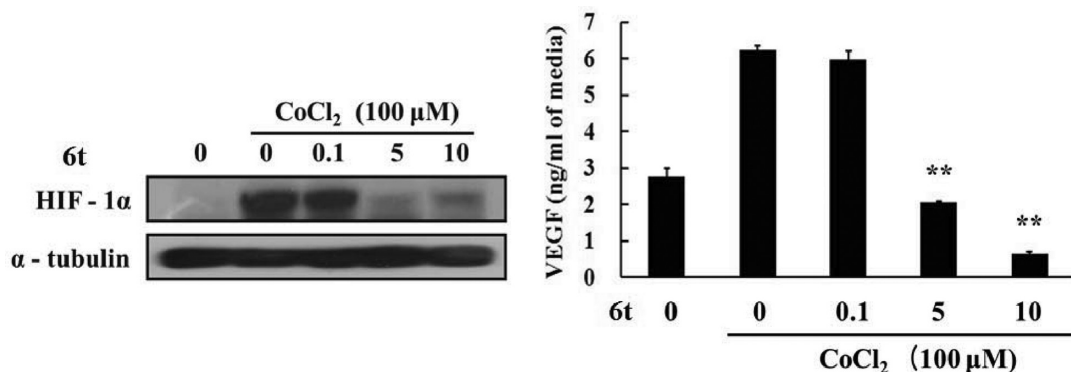


Figure 5. Effect of **6t** on the angiogenesis of MCF-7 breast cancer cells. Effect on the expression of HIF-1 α and production of VEGF by **6t** in hypoxia-induced MCF-7 breast cancer cells (CoCl₂, 100 μ M). Data compared to CoCl₂ from three independent experiments are represented as the mean \pm SD: (**) $P < 0.01$.

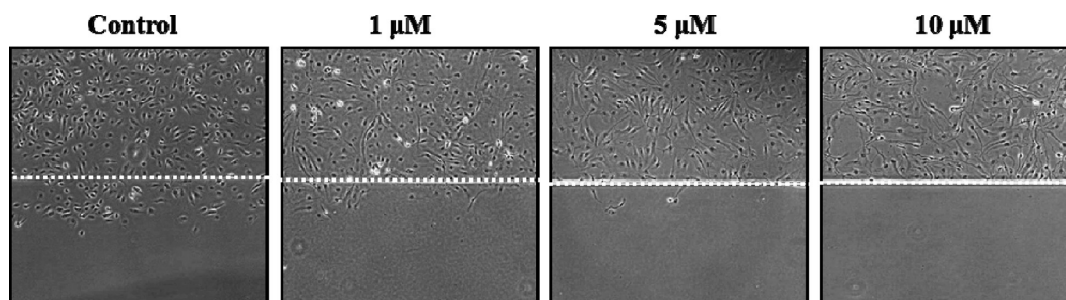


Figure 6. Effects of **6t** on cell migration. HUVECs were plated at 90% confluence and then scratched with a razor blade. Inhibition of HUVEC migration by **6t** in the wound-induced migration assay.

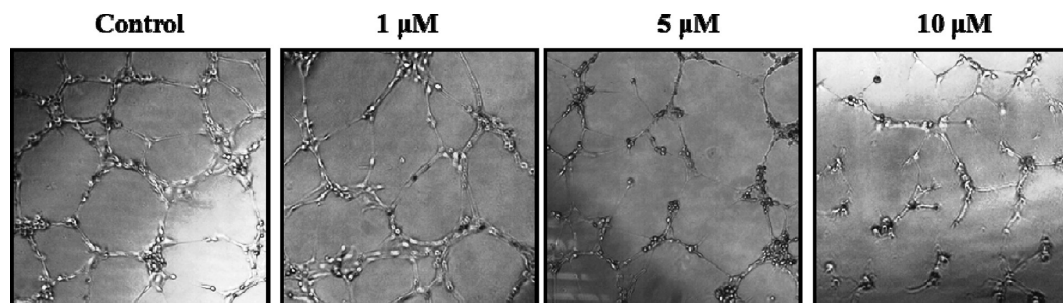


Figure 7. Effect of **6t** on tube formation. Representative images depicting the formation of a HUVEC capillary-like tubular network by treatment with compound **6t** (1, 5, and 10 μ M) and DMSO (control).

CONCLUSION

Utilizing the structural-based design strategy, we designed and synthesized a series of new 7-azaindole derivatives to be used as potent Trk inhibitors. Through the systematic exploration of the appropriate functional groups to place in the C3 and C5 positions of 7-azaindole scaffolds, we successfully developed a SAR profile around the series and found that a 4-pyridyl group at the C3 position and a selection of moieties (e.g., 5-sulfonamide, amide, and oxyethaneamine on aniline ring) at the C5 position of the 7-azaindole scaffold profoundly influenced Trk binding affinity and resulted in nanomolar inhibitors with good antiproliferative cellular activity. Moreover, compound **6t** exhibited strong apoptotic and antiangiogenic effects by inhibiting HIF-1 α and VEGF expression. These results suggest that compound **6t** represses the angiogenic process by inhibiting endothelial cell migration and tube formation.

EXPERIMENTAL SECTION

General Chemistry. Unless stated otherwise, reactions were performed in flame-dried glassware under a positive pressure of nitrogen using freshly distilled solvents. Analytical thin layer chromatography (TLC) was performed on precoated silica gel 60 F₂₅₄ plates, and visualization on TLC was achieved by UV light (254 and 354 nm). Flash column chromatography was undertaken on silica gel (400–630 mesh). ¹H NMR was recorded on 400 or 300 MHz, and chemical shifts were quoted in parts per million (ppm) referenced to the appropriate solvent peak or 0.0 ppm for tetramethylsilane. The following abbreviations were used to describe peak splitting patterns when appropriate: br = broad, s = singlet, d = doublet, t = triplet, q = quartet, m = multiplet, dd = doublet of doublet. Coupling constants, *J*, were reported in hertz unit (Hz). Chemical shifts were reported in ppm referenced to the center line of a triplet at 77.0 ppm of chloroform-*d*. Mass spectral data were obtained from the KAIST Basic Science Institute by using the EI method. High performance liquid chromatography analyses for checking purity (>95% area) of synthesized compounds were performed on Waters HPLC instrument equipped with an Agilent Prep-C18 reverse phase column (21.2 mm \times

150 mm, 10 μ m) and by HRMS. The mobile phase was a mixture of MeOH (0.1% TFA) and H₂O (0.1% TFA). Compound purity was determined by integrating peak areas of the liquid chromatogram, monitored at 254 nm. Parameters were as follows: flow rate of 8 mL/min; gradient system, from 10% MeOH (0.1% TFA) and 90% H₂O (0.1% TFA) (0 min) to 90% MeOH (0.1% TFA) and 10% H₂O (0.1% TFA) (15 min). The solvent ratio was maintained for 18 min. The solvent ratio was then changed to 10% MeOH (0.1% TFA) and 90% H₂O (0.1% TFA) (20 min). All final compounds were found to have >95% purity. Commercial grade reagents and solvents were used without further purification except as indicated below. Dichloromethane was distilled from calcium hydride. THF was distilled from sodium. Unless otherwise stated, all commercial reagents and solvents were used without additional purification.

General Procedure (GP I) for Suzuki Coupling. 5-(3-(3,4-Dimethoxyphenyl)-1H-pyrrolo[2,3-b]pyridin-5-yl)pyridin-3-amine (5c). A solution of 5-bromo-3-(3,4-dimethoxyphenyl)-1H-pyrrolo[2,3-b]pyridine (129 mg, 0.387 mmol), 5-(4,4,5,5-tetramethyl-1,3,2-dioxaborolan-2-yl)pyridin-3-amine (121 mg, 0.548 mmol), K₂CO₃ (158 mg, 1.14 mmol), and PdCl₂(dppf)·CH₂Cl₂ (64 mg, 0.04 mmol) in 1,4-dioxane/H₂O = 3:1 (2 mL) was heated to 100 °C for 5 h under an atmosphere of N₂. The reaction mixture was cooled to room temperature and concentrated in vacuo. The residue was diluted with CH₂Cl₂ and MeOH (10:1, 2 mL) and then filtered through a short plug of silica (SiO₂) and Celite, eluting with CH₂Cl₂ and MeOH (20:1). The filtrate was purified with flash column chromatography (CH₂Cl₂/MeOH, gradient 40:1 to 10:1) to give the product as a white solid (71 mg, 53% yield). ¹H NMR (300 MHz, CDCl₃) δ 3.78 (s, 2H), 3.93 (s, 3H), 3.94 (s, 3H), 6.98 (d, *J* = 7.9 Hz, 1H), 7.13 (s, 1H), 7.19 (s, 1H), 7.21–7.23 (m, 1H), 7.47 (d, *J* = 2.1 Hz, 1H), 8.10 (d, *J* = 2.3 Hz, 1H), 8.30 (s, 2H), 8.54 (s, 1H), 9.20 (s, 1H). HRMS (EI+) *m/z* calcd for C₂₀H₁₈N₄O₂ [M + H]⁺, 347.1508; found 347.1508.

N-(3-(3-(3,4-Dimethoxyphenyl)-1H-pyrrolo[2,3-b]pyridin-5-yl)-phenyl)benzenesulfonamide (5a). Benzenesulfonyl chloride (32 μ L, 0.25 mmol) and pyridine (44 μ L, 0.54 mmol) were added to 5c (65 mg, 0.18 mmol) in CH₂Cl₂ (1.5 mL) under an atmosphere of N₂. The reaction mixture was stirred for 5 h at room temperature, and then the solvent was evaporated. The residue was purified with flash column chromatography (CH₂Cl₂/MeOH = 15:1) to give the product as a pale yellow solid (24 mg, 28% yield). ¹H NMR (300 MHz, DMSO-*d*₆) δ 3.85 (s, 3H), 3.79 (s, 3H), 7.04 (d, *J* = 8.9 Hz, 1H), 7.26–7.28 (m, 2H), 7.55–7.59 (m, 3H), 7.72 (s, 1H), 7.81 (d, *J* = 7.5 Hz, 2H), 7.86 (d, *J* = 2.5 Hz, 1H), 8.25 (d, *J* = 2.3 Hz, 1H), 8.29 (d, *J* = 2.0 Hz, 1H), 8.43 (d, *J* = 2.0 Hz, 1H), 8.63 (s, 1H), 10.69 (s, 1H), 11.99 (s, 1H). HRMS (EI+) *m/z* calcd for C₂₆H₂₂N₄O₄S [M + Na]⁺, 509.1259; found, 509.1267.

N-(3-(3-(3,4-Dimethoxyphenyl)-1H-pyrrolo[2,3-b]pyridin-5-yl)-phenyl)benzenesulfonamide (5b). Compound 5b was prepared (2.4 mg, 28% yield) according to the procedure of benzenesulfonylation (the same as 5a) from 5d (6.0 mg, 0.02 mmol). ¹H NMR (300 MHz, CD₃OD) δ 3.82 (s, 3H), 3.85 (s, 3H), 6.96–6.99 (m, 1H), 7.01–7.16 (m, 3H), 7.28–7.32 (m, 3H), 7.41–7.46 (m, 3H), 7.53 (s, 1H), 7.78 (dd, *J* = 8.2, 1.3 Hz, 2H), 8.18 (d, *J* = 2.1 Hz, 1H), 8.29 (d, *J* = 2.0 Hz, 1H). HRMS (EI+) *m/z* calcd for C₂₇H₂₃N₄O₄S [M + Na]⁺, 508.1307; found, 508.1292.

3-(3-(3,4-Dimethoxyphenyl)-1H-pyrrolo[2,3-b]pyridin-5-yl)aniline (5d). Compound 5d was prepared (11 mg, 25% yield) according to GP I from 3-aminophenylboronic acid (20 mg, 0.15 mmol) and 5-(3-(3,4-dimethoxyphenyl)-1H-pyrrolo[2,3-b]pyridin-5-yl)pyridin-3-amine (40 mg, 0.12 mmol). ¹H NMR (300 MHz, CD₃OD) δ 3.87 (s, 3H), 3.90 (s, 3H), 6.68–6.75 (m, 1H), 6.93–7.06 (m, 3H), 7.20–7.26 (m, 3H), 7.59 (s, 1H), 8.26 (d, *J* = 2.0 Hz, 1H), 8.43 (d, *J* = 2.0 Hz, 1H). HRMS (EI+) *m/z* calcd for C₂₁H₁₉N₃O₂ [M + H]⁺, 346.1556; found, 346.1543.

3-(3-(3,4-Dimethoxyphenyl)-1H-pyrrolo[2,3-b]pyridin-5-yl)-benzotrile (5e). Compound 5e was prepared (6.4 mg, 15% yield) according to GP I from 3-cyanophenylboronic acid (20 mg, 0.14 mmol) and 5-(3-(3,4-dimethoxyphenyl)-1H-pyrrolo[2,3-b]pyridin-5-yl)pyridin-3-amine (40 mg, 0.12 mmol). ¹H NMR (300 MHz, CDCl₃) δ 3.94 (s, 3H), 3.95 (s, 3H), 7.00 (d, *J* = 8.3 Hz, 1H), 7.11 (d, *J* = 1.9

Hz, 1H), 7.22 (dd, *J* = 8.2, 2.0 Hz, 1H), 7.54 (d, *J* = 2.4 Hz, 1H), 7.59 (d, *J* = 7.7 Hz, 1H), 7.63–7.64 (m, 1H), 7.85–7.91 (m, 2H), 8.32 (d, *J* = 2.0 Hz, 1H), 8.57 (d, *J* = 2.0 Hz, 1H), 10.12 (s, 1H). HRMS (EI+) *m/z* calcd for C₂₂H₁₇N₃O₂ [M + Na]⁺, 378.1218; found, 378.1217.

General Procedure (GP II) for Suzuki Coupling. 5-Bromo-3-(3,4-dimethoxyphenyl)-1H-pyrrolo[2,3-b]pyridine. A solution of 5-bromo-3-iodo-1-(phenylsulfonyl)-1H-pyrrolo[2,3-b]pyridine (315 mg, 0.680 mmol), dimethoxyboronic acid (124 mg, 0.680 mmol), K₂CO₃ (282 mg, 2.04 mmol), and PdCl₂(dppf)·CH₂Cl₂ (111 mg, 0.136 mmol) in 1,4-dioxane/H₂O = 3:1 (4 mL) was heated to 80 °C for 3 h under an atmosphere of N₂. The resulting solution was cooled to room temperature, and 6 N KOH solution (2 mL) was added. The reaction mixture was then heated to 80 °C and stirred for 30 min (N-deprotection of benzenesulfonyl group). The mixture was diluted with water and neutralized with 6 N HCl solution. The two-phase mixture was extracted with CH₂Cl₂. The combined organic layer was dried (MgSO₄) and concentrated in vacuo. The residue was purified with flash column chromatography (CH₂Cl₂/MeOH, gradient 40:1 to 10:1) to give the product as a yellow solid (178 mg, 78.6% yield). ¹H NMR (300 MHz, CDCl₃) δ 3.91 (s, 3H), 3.93 (s, 3H), 6.91–6.95 (m, 1H), 7.03–7.08 (m, 2H), 7.41 (s, 1H), 8.23 (s, 1H), 8.32 (s, 1H), 11.25 (s, 1H).

3-(3-(Pyridin-4-yl)-1H-pyrrolo[2,3-b]pyridin-5-yl)aniline (5f). 5-Bromo-3-(pyridin-4-yl)-1H-pyrrolo[2,3-b]pyridine was prepared (243 mg, 53.3% yield) according to GP II from 4-pyridinylboronic acid (398 mg, 3.24 mmol) and 5-bromo-3-iodo-1-(phenylsulfonyl)-1H-pyrrolo[2,3-b]pyridine (1.50 g, 3.24 mmol). ¹H NMR (300 MHz, DMSO-*d*₆) δ 7.97 (d, *J* = 5.9 Hz, 2H), 8.41 (d, *J* = 2.2 Hz, 1H), 8.47 (d, *J* = 2.7 Hz, 1H), 8.60 (d, *J* = 6.0 Hz, 2H), 8.70 (d, *J* = 2.1 Hz, 1H), 12.69 (s, 1H). Compound 5f was prepared (11 mg, 42% yield) according to GP I from 3-aminophenylboronic acid (23 mg, 0.17 mmol) and 5-bromo-3-(pyridin-4-yl)-1H-pyrrolo[2,3-b]pyridine (39 mg, 0.14 mmol). ¹H NMR (300 MHz, DMSO-*d*₆) δ 5.18 (s, 2H), 6.59 (d, *J* = 7.8 Hz, 1H), 6.90 (d, *J* = 7.7 Hz, 1H), 6.93 (s, 1H), 7.14 (t, *J* = 7.7 Hz, 1H), 7.81 (d, *J* = 6.0 Hz, 2H), 8.25 (s, 1H), 8.45 (d, *J* = 1.8 Hz, 1H), 8.50 (d, *J* = 1.7 Hz, 1H), 8.56 (d, *J* = 5.9 Hz, 2H), 12.28 (s, 1H). ¹³C NMR (100 MHz, DMSO-*d*₆) δ 111.6, 112.6, 112.9, 114.9, 116.9, 120.4, 125.3, 127.0, 129.5, 130.3, 139.4, 142.3, 142.4, 148.7, 149.2, 145.0. HRMS (EI+) *m/z* calcd for C₁₈H₁₄N₄ [M + H]⁺, 287.1297; found, 287.1289.

3-(3-(Pyridin-3-yl)-1H-pyrrolo[2,3-b]pyridin-5-yl)aniline (5g). 5-Bromo-3-(pyridin-3-yl)-1H-pyrrolo[2,3-b]pyridine was prepared (35 mg, 30% yield) according to GP II from 3-pyridinylboronic acid (53 mg, 0.43 mmol) and 5-bromo-3-iodo-1-(phenylsulfonyl)-1H-pyrrolo[2,3-b]pyridine (0.20 g, 0.43 mmol). ¹H NMR (300 MHz, CD₃OD) δ 7.46 (dd, *J* = 4.9, 7.2 Hz, 1H), 7.80 (s, 1H), 8.05–8.09 (m, 1H), 8.28 (d, *J* = 2.1 Hz, 1H), 8.36 (d, *J* = 2.1 Hz, 1H), 8.39 (dd, *J* = 1.6, 4.9 Hz, 1H), 8.78 (dd, *J* = 0.75, 2.2 Hz, 1H). Compound 5g was prepared (11 mg, 30% yield) according to GP I from 3-aminophenylboronic acid (35 mg, 0.15 mmol) and 5-bromo-3-(pyridin-3-yl)-1H-pyrrolo[2,3-b]pyridine (35 mg, 0.13 mmol). ¹H NMR (300 MHz, CD₃OD) δ 6.78 (d, *J* = 7.5 Hz, 1H), 7.03 (d, *J* = 7.6, 1H), 7.08 (d, *J* = 1.8 Hz, 1H), 7.25 (t, *J* = 7.8 Hz, 1H), 7.54–7.57 (m, 1H), 7.87 (s, 1H), 8.22–8.25 (m, 1H), 8.42–8.54 (m, 3H), 8.94 (d, *J* = 1.7 Hz, 1H). HRMS (EI+) *m/z* calcd for C₁₈H₁₄N₄ [M + Na]⁺, 309.1116; found, 309.1117.

3-(3-Phenyl-1H-pyrrolo[2,3-b]pyridin-5-yl)aniline (5h). 5-Bromo-3-phenyl-1H-pyrrolo[2,3-b]pyridine was prepared (41 mg, 58% yield) according to GP II from phenylboronic acid (30 mg, 0.24 mmol) and 5-bromo-3-iodo-1-(phenylsulfonyl)-1H-pyrrolo[2,3-b]pyridine (113 mg, 0.24 mmol). ¹H NMR (300 MHz, DMSO-*d*₆) δ 7.26 (t, *J* = 7.4 Hz, 1H), 7.41–7.46 (m, 2H), 7.69–7.72 (m, 2H), 7.95 (s, 1H), 8.32 (d, *J* = 2.1 Hz, 1H), 8.43 (d, *J* = 2.1 Hz, 1H), 12.17 (s, 1H). Compound 5h was prepared (24 mg, 56% yield) according to GP I from 3-aminophenylboronic acid (24 mg, 0.16 mmol) and 5-bromo-3-phenyl-1H-pyrrolo[2,3-b]pyridine (41 mg, 0.15 mmol). ¹H NMR (300 MHz, DMSO-*d*₆) δ 5.15 (s, 2H), 6.56 (d, *J* = 7.9 Hz, 1H), 6.85 (d, *J* = 7.2 Hz, 1H), 6.90 (s, 1H), 7.12 (t, *J* = 7.8 Hz, 1H), 7.23–7.28 (m, 1H), 7.42–7.47 (m, 2H), 7.75 (d, *J* = 7.2 Hz, 2H), 7.88 (d, *J* = 2.5 Hz, 1H), 8.30 (d, *J* = 2.0 Hz, 1H), 8.46 (d, *J* = 2.0 Hz, 1H), 11.95 (s, 1H). ¹³C NMR (100 MHz, DMSO-*d*₆) δ 112.5, 112.7, 114.5, 114.7, 117.2, 124.4, 124.9, 125.7, 126.4, 128.9, 129.5, 129.6, 135.0, 139.6, 141.8,

148.5, 149.2. HRMS (EI+) m/z calcd for $C_{19}H_{15}N_3$ $[M + H]^+$, 286.1344; found, 286.1346.

3-(5-(3-Aminophenyl)-1H-pyrrolo[2,3-b]pyridin-3-yl)benzoxazole (5i). 3-(5-Bromo-1H-pyrrolo[2,3-b]pyridin-3-yl)benzoxazole was prepared (54 mg, 84% yield) according to GP II from 3-cyanophenylboronic acid (33 mg, 0.22 mmol) and 5-bromo-3-iodo-1-(phenylsulfonyl)-1H-pyrrolo[2,3-b]pyridine (100 mg, 0.216 mmol). 1H NMR (300 MHz, DMSO- d_6) δ 7.59–7.70 (m, 2H), 8.07–8.19 (m, 3H), 8.35 (d, $J = 2.1$ Hz, 1H), 8.59 (d, $J = 2.1$ Hz, 1H), 12.38 (s, 1H). Compound 5i was prepared (16 mg, 39% yield) according to GP I from 3-aminophenylboronic acid (21 mg, 0.15 mmol) and 3-(5-bromo-1H-pyrrolo[2,3-b]pyridin-3-yl)benzoxazole (40 mg, 0.13 mmol). 1H NMR (300 MHz, CD $_3$ OD) δ 6.73 (dd, $J = 8.0, 1.3$ Hz, 1H), 6.96–7.03 (m, 2H), 7.20 (t, $J = 7.8$ Hz, 1H), 7.58–7.60 (m, 2H), 7.78 (s, 1H), 7.99–8.01 (m, 2H), 8.35 (d, $J = 2.0$ Hz, 1H), 8.46 (d, $J = 1.9$ Hz, 1H). HRMS (EI+) m/z calcd for $C_{20}H_{14}N_4$ $[M + Na]^+$, 333.1116; found, 333.1101.

3-(3-(3-Aminophenyl)-1H-pyrrolo[2,3-b]pyridin-5-yl)benzoxazole (5j). 3-(5-Bromo-1H-pyrrolo[2,3-b]pyridin-3-yl)aniline was prepared (158 mg, 50.9% yield) according to GP II from 3-aminophenylboronic acid (237 mg, 1.08 mmol) and 5-bromo-3-iodo-1-(phenylsulfonyl)-1H-pyrrolo[2,3-b]pyridine (500 mg, 1.08 mmol). 1H NMR (300 MHz, CD $_3$ OD) δ 6.65–6.68 (m, 1H), 6.90–7.00 (m, 2H), 7.23–7.48 (m, 1H), 7.48 (d, $J = 2.5$ Hz, 1H), 8.35 (d, $J = 2.0$ Hz, 1H), 8.39 (d, $J = 2.1$ Hz, 1H), 9.71 (s, 1H). Compound 5j was prepared (25 mg, 26% yield) according to GP I from 3-cyanophenylboronic acid (51 mg, 0.35 mmol) and 3-(5-bromo-1H-pyrrolo[2,3-b]pyridin-3-yl)aniline (91 mg, 0.32 mmol). 1H NMR (300 MHz, DMSO- d_6) δ 5.09 (s, 2H), 6.49 (d, $J = 7.9$ Hz, 1H), 6.92 (d, $J = 7.7$ Hz, 1H), 7.02 (s, 1H), 7.09 (t, $J = 7.7$ Hz, 1H), 7.70 (t, $J = 7.8$ Hz, 1H), 7.78 (s, 1H), 7.83 (d, $J = 7.8$ Hz, 1H), 8.14 (d, $J = 8.0$ Hz, 1H), 8.28 (s, 1H), 8.48 (d, $J = 2.2$ Hz, 1H), 8.61 (d, $J = 2.1$ Hz, 1H), 11.97 (s, 1H). ^{13}C NMR (100 MHz, DMSO- d_6) δ 111.8, 112.1, 112.1, 114.4, 115.7, 117.4, 118.9, 124.3, 126.0, 126.5, 129.4, 130.1, 130.5, 130.5, 131.9, 135.1, 140.4, 141.9, 148.9, 149.0. HRMS (EI+) m/z calcd for $C_{20}H_{14}N_4$ $[M + Na]^+$, 333.1116; found, 333.1098.

5-(3-(Pyridin-4-yl)-1H-pyrrolo[2,3-b]pyridin-5-yl)pyridin-3-amine (6a). Compound 6a was prepared (10 mg, 28% yield) according to GP I from 5-(4,4,5,5-tetramethyl-1,3,2-dioxaborolan-2-yl)pyridin-3-amine (42 mg, 0.19 mmol) and 5-bromo-3-(pyridin-4-yl)-1H-pyrrolo[2,3-b]pyridine (35 mg, 0.13 mmol). 1H NMR (300 MHz, DMSO- d_6) δ 5.40 (s, 2H), 7.25 (t, $J = 7.25$ Hz, 1H), 7.83 (dd, $J = 4.6, 1.6$ Hz, 2H), 7.95 (d, $J = 4.3$ Hz, 1H), 8.15 (d, $J = 2.0$ Hz, 1H), 8.26 (s, 1H), 8.52 (s, 2H), 8.55 (dd, $J = 4.6, 1.5$ Hz, 2H), 12.38 (s, 1H). HRMS (EI+) m/z calcd for $C_{17}H_{13}N_5$ $[M + Na]^+$, 310.1069; found, 310.1065.

General Procedure (GP III) for Suzuki Coupling. N-Methyl-3-(3-(pyridin-4-yl)-1H-pyrrolo[2,3-b]pyridin-5-yl)aniline (6b). 5-Bromo-1-(phenylsulfonyl)-3-(pyridin-4-yl)-1H-pyrrolo[2,3-b]pyridine was prepared from 4-pyridinylboronic acid and 5-bromo-3-iodo-1-(phenylsulfonyl)-1H-pyrrolo[2,3-b]pyridine (73% yield) according to the procedure of GP II without N-deprotection step of benzenesulfonyl group. 1H NMR (300 MHz, DMSO- d_6) δ 7.62–7.67 (m, 2H), 7.73–7.78 (m, 1H), 7.85–7.87 (m, 2H), 8.15–8.18 (m, 2H), 8.56 (d, $J = 2.1$ Hz, 1H), 8.62–8.65 (m, 3H), 8.67 (d, $J = 2.2$ Hz, 1H). A solution of 5-bromo-1-(phenylsulfonyl)-3-(pyridin-4-yl)-1H-pyrrolo[2,3-b]pyridine (1.0 g, 2.24 mmol), bis(pinacolato)diboron (685 mg, 2.69 mmol), KOAc (660 mg, 6.72 mmol), and PdCl $_2$ (dppf)·CH $_2$ Cl $_2$ (183 mg, 0.224 mmol) in anhydrous 1,4-dioxane was heated to 100 °C for 12 h under an atmosphere of N $_2$. The reaction mixture was cooled to room temperature and concentrated in vacuo. The residue was diluted with CH $_2$ Cl $_2$ and MeOH and then filtered through a short pad of silica (SiO $_2$) and Celite, eluting with CH $_2$ Cl $_2$ and MeOH (30:1). The filtrate was concentrated in vacuo to give the crude compound 4 as a brown solid (590 mg, 57.1% yield). The crude product was used for the next Suzuki coupling without further purification. A solution of 3-bromo-N-methylaniline (25 mg, 0.13 mmol), compound 4 (78 mg, 0.17 mmol), K $_2$ CO $_3$ (54 mg, 0.39 mmol), and PdCl $_2$ (dppf)·CH $_2$ Cl $_2$ (10 mg, 0.012 mmol) in 1,4-dioxane/H $_2$ O = 3:1 (2 mL) was heated to 100 °C for 5 h under an atmosphere of N $_2$. The resulting solution was cooled to room temperature, and 6 N KOH solution (2 mL) was

added. The reaction mixture was then heated to about 80 °C and stirred for 30 min (N-deprotection of benzenesulfonyl group). The mixture was diluted with water and neutralized with 6 N HCl solution. All solvent was removed in vacuum. The residue was dissolved into CH $_2$ Cl $_2$ /MeOH = 5:1, and an insoluble salt was removed by filtration. The filtrate was concentrated and purified with flash column chromatography (CH $_2$ Cl $_2$ /MeOH, gradient 30:1 to 10:1) to give the product as a yellow solid (13 mg, 45% yield). 1H NMR (300 MHz, DMSO- d_6) δ 2.75 (d, $J = 5.0$ Hz, 3H), 5.72–5.75 (m, 1H), 6.57 (d, $J = 7.8$ Hz, 1H), 6.86 (s, 1H), 6.92 (d, $J = 7.7$ Hz, 1H), 7.20 (t, $J = 7.8$ Hz, 1H), 7.81 (d, $J = 6.0$ Hz, 2H), 8.24 (s, 1H), 8.47 (d, $J = 1.9$ Hz, 1H), 8.53 (d, $J = 1.8$ Hz, 1H), 8.56 (d, $J = 6.0$ Hz, 2H), 12.27 (s, 1H). ^{13}C NMR (100 MHz, DMSO- d_6) δ 29.8, 110.5, 110.5, 111.7, 114.8, 116.9, 120.4, 125.5, 127.02, 129.5, 130.4, 139.5, 142.3, 142.4, 148.7, 150.0, 150.4. HRMS (EI+) m/z calcd for $C_{19}H_{16}N_4$ $[M + Na]^+$, 323.1273; found, 323.1252.

N,N-Dimethyl-3-(3-(pyridin-4-yl)-1H-pyrrolo[2,3-b]pyridin-5-yl)aniline (6c). Compound 6c was prepared (7.2 mg, 18% yield) according to GP I from 3-(dimethylamino)phenylboronic acid (26 mg, 0.16 mmol) and 5-bromo-3-(pyridin-4-yl)-1H-pyrrolo[2,3-b]pyridine (35 mg, 0.13 mmol). 1H NMR (300 MHz, CDCl $_3$) δ 3.03 (s, 6H), 6.77–6.94 (m, 1H), 6.94–6.99 (m, 2H), 7.36 (t, $J = 7.7$ Hz, 1H), 7.59 (dd, $J = 4.6, 1.6$ Hz, 2H), 7.78 (s, 1H), 8.44 (d, $J = 1.9$ Hz, 1H), 8.63–8.65 (m, 3H), 11.30 (s, 1H). HRMS (EI+) m/z calcd for $C_{20}H_{18}N_4$ $[M + H]^+$, 315.1610; found, 315.1613.

5-(3-(Methoxyphenyl)-3-(pyridin-4-yl)-1H-pyrrolo[2,3-b]pyridine (6d). Compound 6d was prepared (10 mg, 35% yield) according to GP I from 3-methoxyphenylboronic acid (22 mg, 0.14 mmol) and 5-bromo-3-(pyridin-4-yl)-1H-pyrrolo[2,3-b]pyridine (26 mg, 0.09 mmol). 1H NMR (300 MHz, CD $_3$ OD) δ 3.89 (s, 3H), 6.96 (dd, $J = 7.8, 1.8$ Hz, 1H), 7.22–7.27 (m, 2H), 7.41 (t, $J = 7.9$ Hz, 1H), 7.80 (dd, $J = 4.7, 1.5$ Hz, 2H), 8.02 (s, 1H), 8.52–8.54 (m, 4H). ^{13}C NMR (100 MHz, DMSO- d_6) δ 55.2, 111.8, 112.6, 112.9, 117.0, 119.6, 120.4, 125.8, 127.2, 129.3, 130.0, 140.3, 142.3, 142.5, 148.9, 150.0, 159.8. HRMS (EI+) m/z calcd for $C_{19}H_{15}N_3O$ $[M + Na]^+$, 324.1113; found, 324.1113.

N-(3-(3-(Pyridin-4-yl)-1H-pyrrolo[2,3-b]pyridin-5-yl)phenyl)acetamide (6e). Compound 6e was prepared (5.7 mg, 12% yield) according to GP I from N-(3-(4,4,5,5-tetramethyl-1,3,2-dioxaborolan-2-yl)phenyl)acetamide (50 mg, 0.19 mmol) and 5-bromo-3-(pyridin-4-yl)-1H-pyrrolo[2,3-b]pyridine (40 mg, 0.15 mmol). 1H NMR (300 MHz, DMSO- d_6) δ 2.07 (s, 3H), 7.38–7.50 (m, 2H), 7.66 (d, $J = 7.5$ Hz, 1H), 7.82 (d, $J = 5.7$ Hz, 2H), 7.88 (s, 1H), 8.27 (d, $J = 2.7$ Hz, 1H), 8.51–8.57 (m, 4H), 10.06 (s, 1H), 12.33 (s, 1H). ^{13}C NMR (100 MHz, DMSO- d_6) δ 24.1, 111.7, 117.0, 117.7, 117.8, 120.5, 122.0, 125.6, 127.4, 129.3, 129.5, 139.2, 139.9, 142.3, 142.5, 148.9, 149.8, 168.4. HRMS (EI+) m/z calcd for $C_{20}H_{16}N_4O$ $[M + H]^+$, 329.1402; found, 329.1399.

4-(3-(Pyridin-4-yl)-1H-pyrrolo[2,3-b]pyridin-5-yl)aniline (6f). Compound 6f was prepared (8.3 mg, 27% yield) according to GP I from 4-aminophenylboronic acid pinacol ester (30 mg, 0.14 mmol) and 5-bromo-3-(pyridin-4-yl)-1H-pyrrolo[2,3-b]pyridine (29 mg, 0.11 mmol). 1H NMR (300 MHz, DMSO- d_6) δ 5.20 (s, 2H), 6.68 (d, $J = 8.4$ Hz, 2H), 7.46 (d, $J = 8.3$ Hz, 2H), 7.81 (d, $J = 6.2$ Hz, 2H), 8.19 (d, $J = 2.8$ Hz, 1H), 8.40 (s, 1H), 8.48 (s, 1H), 8.54 (d, $J = 6.0$ Hz, 2H), 12.17 (s, 1H). HRMS (EI+) m/z calcd for $C_{18}H_{14}N_4$ $[M + H]^+$, 287.1297; found, 287.1295.

2-Methoxy-5-(3-(pyridin-4-yl)-1H-pyrrolo[2,3-b]pyridin-5-yl)aniline (6g). Compound 6g was prepared (5.9 mg, 11% yield) according to GP III from 5-bromo-2-methoxyaniline (35 mg, 0.17 mmol). 1H NMR (300 MHz, DMSO- d_6) δ 3.80 (s, 3H), 4.81 (s, 2H), 6.88–6.95 (m, 2H), 7.02 (d, $J = 1.7$ Hz, 1H), 7.79 (d, $J = 6.1$ Hz, 2H), 8.21 (s, 1H), 8.40 (d, $J = 1.9$ Hz, 1H), 8.47 (d, $J = 1.9$ Hz, 1H), 8.55 (d, $J = 6.0$ Hz, 2H), 12.22 (s, 1H). HRMS (EI+) m/z calcd for $C_{19}H_{16}N_4O$ $[M + H]^+$, 317.1402; found, 317.1384.

2-Chloro-5-(3-(pyridin-4-yl)-1H-pyrrolo[2,3-b]pyridin-5-yl)aniline (6h). Compound 6h was prepared (5.6 mg, 15% yield) according to GP III from 5-bromo-2-chloroaniline (24 mg, 0.12 mmol). 1H NMR (300 MHz, DMSO- d_6) δ 5.24 (s, 2H), 6.96 (dd, $J = 8.1, 1.7$ Hz, 1H), 7.17 (d, $J = 1.7$ Hz, 1H), 7.29 (d, $J = 8.3$ Hz, 1H), 7.80 (d, $J = 5.6$ Hz,

2H), 8.24 (s, 1H), 8.46 (s, 1H), 8.49 (s, 1H), 8.55 (d, $J = 5.6$ Hz, 2H), 12.30 (s, 1H). ^{13}C NMR (100 MHz, DMSO- d_6) δ 111.7, 113.9, 115.9, 116.4, 116.9, 120.4, 125.4, 127.2, 129.1, 129.4, 138.3, 142.1, 142.3, 145.0, 148.8, 150.0. HRMS (EI+) m/z calcd for $\text{C}_{18}\text{H}_{13}\text{Cl}_3\text{N}_4$ [$\text{M} + \text{H}$] $^+$, 321.0907; found, 321.0924.

2-Methyl-5-(3-(pyridin-4-yl)-1H-pyrrolo[2,3-b]pyridin-5-yl)aniline (6i). Compound **6i** was prepared (12 mg, 28% yield) according to GP I from 2-methyl-5-(4,4,5,5-tetramethyl-1,3,2-dioxaborolan-2-yl)aniline (51 mg, 0.22 mmol) and 5-bromo-3-(pyridin-4-yl)-1H-pyrrolo[2,3-b]pyridine (40 mg, 0.15 mmol). ^1H NMR (300 MHz, CD_3OD) δ 2.17 (s, 3H), 6.91 (dd, $J = 7.7, 1.8$ Hz, 1H), 7.03 (d, $J = 1.7$ Hz, 1H), 7.07 (d, $J = 7.7$ Hz, 1H), 7.75 (d, $J = 4.8, 1.4$ Hz, 2H), 7.96 (s, 1H), 8.45–8.48 (m, 4H). ^{13}C NMR (100 MHz, DMSO- d_6) δ 17.1, 111.6, 112.6, 115.0, 117.0, 120.3, 120.4, 125.0, 127.0, 130.2, 130.5, 136.9, 142.2, 142.4, 147.0, 148.6, 150.0. HRMS (EI+) m/z calcd for $\text{C}_{19}\text{H}_{16}\text{N}_4$ [$\text{M} + \text{Na}$] $^+$, 323.1273; found, 323.1267.

(2-Amino-4-(3-(pyridin-4-yl)-1H-pyrrolo[2,3-b]pyridin-5-yl)phenyl)(morpholino)methanone (6j). Compound **6j** was prepared (10 mg, 13% yield) according to GP III from (2-amino-4-bromophenyl)(morpholino)methanone (34 mg, 0.12 mmol). ^1H NMR (300 MHz, CDCl_3) δ 3.70–3.72 (m, 8H), 4.53 (s, 2H), 6.97–6.99 (m, 2H), 7.20 (d, $J = 8.3$ Hz, 1H), 7.58 (d, $J = 5.5$ Hz, 2H), 7.72 (s, 1H), 8.38 (s, 1H), 8.59 (s, 1H), 8.65 (d, $J = 5.6$ Hz, 2H), 9.55 (s, 1H). HRMS (EI+) m/z calcd for $\text{C}_{23}\text{H}_{21}\text{N}_5\text{O}_2$ [$\text{M} + \text{H}$] $^+$, 400.1773; found, 400.1808.

2-(2-(Dimethylamino)ethoxy)-5-(3-(pyridin-4-yl)-1H-pyrrolo[2,3-b]pyridin-5-yl)aniline (6k). Compound **6k** was prepared (2.4 mg, 8.3% yield) according to GP III from 5-bromo-2-(2-(dimethylamino)ethoxy)aniline (20 mg, 0.079 mmol). ^1H NMR (300 MHz, CDCl_3) δ 2.35 (s, 6H), 2.77 (t, $J = 6.0$ Hz, 2H), 4.07 (s, 2H), 4.15 (t, $J = 6.0$ Hz, 2H), 6.91–6.96 (m, 2H), 6.96 (s, 1H), 7.56 (d, $J = 5.0$ Hz, 2H), 7.70 (s, 1H), 8.34 (s, 1H), 8.56 (s, 1H), 8.62 (d, $J = 5.1$ Hz, 2H), 10.73 (s, 1H). HRMS (EI+) m/z calcd for $\text{C}_{22}\text{H}_{23}\text{N}_5\text{O}$ [$\text{M} + \text{H}$] $^+$, 374.1981; found, 374.1982.

3-Methoxy-5-(3-(pyridin-4-yl)-1H-pyrrolo[2,3-b]pyridin-5-yl)aniline (6l). Compound **6l** was prepared (5.0 mg, 26% yield) according to GP III from 3-bromo-5-methoxyaniline (12 mg, 0.060 mmol). ^1H NMR (300 MHz, CDCl_3) δ 3.84 (m, 5H), 6.28 (t, $J = 2.0$ Hz, 1H), 6.55 (d, $J = 1.7$ Hz, 1H), 6.57 (d, $J = 1.9$ Hz, 1H), 7.57 (d, $J = 6.1$ Hz, 2H), 7.72 (d, $J = 1.7$ Hz, 1H), 8.39 (d, $J = 1.9$ Hz, 1H), 8.59 (d, $J = 2.0$ Hz, 1H), 8.64 (d, $J = 6.1$ Hz, 2H), 10.02 (s, 1H). HRMS (EI+) m/z calcd for $\text{C}_{19}\text{H}_{16}\text{N}_4\text{O}$ [$\text{M} + \text{H}$] $^+$, 317.1402; found, 317.1390.

(3-Amino-5-(3-(pyridin-4-yl)-1H-pyrrolo[2,3-b]pyridin-5-yl)phenyl)(morpholino)methanone (6m). Compound **6m** was prepared (11 mg, 19% yield) according to GP III from (3-amino-5-bromophenyl)(morpholino)methanone (39 mg, 0.14 mmol). ^1H NMR (400 MHz, CDCl_3 , 60 °C) δ 3.64–3.67 (m, 8H), 3.85 (s, 2H), 6.70 (dd, $J = 2.2, 1.4$ Hz, 1H), 6.95 (t, $J = 1.8$ Hz, 1H), 7.00 (t, $J = 1.4$ Hz, 1H), 7.54 (d, $J = 4.6$ Hz, 2H), 7.66 (s, 1H), 8.35 (d, $J = 2.0$ Hz, 1H), 8.56 (d, $J = 2.0$ Hz, 1H), 8.65 (d, $J = 4.6$ Hz, 2H), 9.03 (s, 1H). HRMS (EI+) m/z calcd for $\text{C}_{23}\text{H}_{21}\text{N}_5\text{O}_2$ [$\text{M} + \text{H}$] $^+$, 400.1773; found, 400.1752.

3-(2-(Dimethylamino)ethoxy)-5-(3-(pyridin-4-yl)-1H-pyrrolo[2,3-b]pyridin-5-yl)aniline (6n). Compound **6n** was prepared (12 mg, 25% yield) according to GP III from 3-bromo-5-((dimethylamino)methoxy)aniline (26 mg, 0.10 mmol). ^1H NMR (300 MHz, CD_3OD) δ 3.01 (s, 6H), 3.64 (t, $J = 5.0$ Hz, 2H), 4.46 (t, $J = 4.9$ Hz, 2H), 6.76 (t, $J = 1.9$ Hz, 1H), 7.09 (s, 2H), 8.41 (s, 1H), 8.44 (s, 1H), 8.57 (s, 1H), 8.65–8.67 (m, 3H), 8.71 (d, $J = 1.9$ Hz, 1H). HRMS (EI+) m/z calcd for $\text{C}_{22}\text{H}_{23}\text{N}_5\text{O}$ [$\text{M} + \text{H}$] $^+$, 374.1981; found, 374.2013.

3-(2-Morpholinoethoxy)-5-(3-(pyridin-4-yl)-1H-pyrrolo[2,3-b]pyridin-5-yl)aniline (6o). Compound **6o** was prepared (12 mg, 28% yield) according to GP III from 3-bromo-5-(morpholinomethoxy)aniline (31 mg, 0.10 mmol). ^1H NMR (300 MHz, CD_3OD) δ 2.63 (t, $J = 4.6$ Hz, 4H), 2.83 (t, $J = 5.4$ Hz, 2H), 3.72 (t, $J = 4.7$ Hz, 4H), 4.17 (t, $J = 5.4$ Hz, 2H), 6.35 (s, 1H), 6.58 (s, 1H), 6.65 (s, 1H), 7.79 (d, $J = 6.4$ Hz, 2H), 8.01 (s, 1H), 8.48–8.52 (m, 4H). HRMS (EI+) m/z calcd for $\text{C}_{24}\text{H}_{25}\text{N}_5\text{O}_2$ [$\text{M} + \text{H}$] $^+$, 416.2087; found, 416.2086.

N-(3-Amino-5-(3-(pyridin-4-yl)-1H-pyrrolo[2,3-b]pyridin-5-yl)phenyl)methanesulfonamide (6p). Compound **6p** was prepared (10 mg, 18% yield) according to GP I from *N*-(3-amino-5-(4,4,5,5-tetramethyl-1,3,2-dioxaborolan-2-yl)phenyl)methanesulfonamide (65 mg, 0.20 mmol) and 5-bromo-3-(pyridin-4-yl)-1H-pyrrolo[2,3-b]pyridine (42 mg, 0.16 mmol). ^1H NMR (300 MHz, DMSO- d_6) δ 2.99 (s, 3H), 5.34 (s, 2H), 6.51 (s, 1H), 6.66 (s, 2H), 7.77 (d, $J = 6.1$ Hz, 2H), 8.24 (s, 1H), 8.39 (s, 1H), 8.44 (s, 1H), 8.55 (d, $J = 6.0$ Hz, 2H), 12.30 (s, 1H). ^{13}C NMR (100 MHz, DMSO- d_6) δ 48.6, 103.8, 106.5, 108.6, 111.6, 116.9, 120.4, 125.3, 127.2, 130.0, 139.7, 140.2, 142.1, 142.4, 148.8, 150.0, 150.1. HRMS (EI+) m/z calcd for $\text{C}_{19}\text{H}_{17}\text{N}_5\text{O}_2\text{S}$ [$\text{M} + \text{H}$] $^+$, 380.1181; found, 380.1179.

N-(3-Amino-5-(3-(pyridin-4-yl)-1H-pyrrolo[2,3-b]pyridin-5-yl)phenyl)benzenesulfonamide (6q). Compound **6q** was prepared (65 mg, 81% yield) according to GP I from *N*-(3-amino-5-(4,4,5,5-tetramethyl-1,3,2-dioxaborolan-2-yl)phenyl)benzenesulfonamide (103 mg, 0.274 mmol) and 5-bromo-3-(pyridin-4-yl)-1H-pyrrolo[2,3-b]pyridine (50 mg, 0.18 mmol). ^1H NMR (300 MHz, DMSO- d_6) δ 5.26 (s, 2H), 6.43 (s, 1H), 6.52 (s, 1H), 6.56 (s, 1H), 7.53–7.60 (m, 3H), 7.74 (d, $J = 5.9$ Hz, 2H), 7.80 (s, 1H), 7.82 (s, 1H), 8.23 (s, 1H), 8.26 (s, 1H), 8.30 (s, 1H), 8.56 (d, $J = 5.7$ Hz, 2H), 10.13 (s, 1H), 12.25 (s, 1H). ^{13}C NMR (100 MHz, DMSO- d_6) δ 104.1, 106.5, 108.8, 111.6, 116.9, 120.4, 125.1, 126.7, 127.2, 129.1, 129.8, 132.7, 138.9, 139.8, 139.9, 141.9, 142.3, 148.8, 149.9, 150.0. HRMS (EI+) m/z calcd for $\text{C}_{24}\text{H}_{19}\text{N}_5\text{O}_2\text{S}$ [$\text{M} + \text{H}$] $^+$, 442.1338; found, 442.1349.

N-(3-Amino-5-(3-(pyridin-4-yl)-1H-pyrrolo[2,3-b]pyridin-5-yl)phenyl)-4-methylbenzenesulfonamide (6r). Compound **6r** was prepared (21 mg, 49% yield) according to GP I from *N*-(3-amino-5-(4,4,5,5-tetramethyl-1,3,2-dioxaborolan-2-yl)phenyl)-4-methylbenzenesulfonamide (46 mg, 0.12 mmol) and 5-bromo-3-(pyridin-4-yl)-1H-pyrrolo[2,3-b]pyridine (26 mg, 0.095 mmol). ^1H NMR (300 MHz, DMSO- d_6) δ 2.31 (s, 3H), 5.26 (s, 2H), 6.42 (s, 1H), 6.53 (s, 1H), 6.55 (s, 1H), 7.34 (d, $J = 8.2$ Hz, 2H), 7.69 (d, $J = 8.2$ Hz, 2H), 7.75 (d, $J = 6.1$ Hz, 2H), 8.23 (s, 1H), 8.28 (d, $J = 2.0$ Hz, 1H), 8.31 (d, $J = 1.9$ Hz, 1H), 8.56 (d, $J = 6.0$ Hz, 2H), 10.00 (s, 1H), 12.27 (s, 1H). ^{13}C NMR (100 MHz, DMSO- d_6) δ 20.9, 103.8, 106.3, 108.6, 111.6, 116.9, 120.4, 125.1, 126.8, 127.2, 129.6, 129.8, 136.9, 139.1, 139.8, 141.9, 142.3, 143.0, 148.8, 149.9, 150.0. HRMS (EI+) m/z calcd for $\text{C}_{25}\text{H}_{21}\text{N}_5\text{O}_2\text{S}$ [$\text{M} + \text{H}$] $^+$, 456.1494; found, 456.1476.

N-(3-Amino-5-(3-(pyridin-4-yl)-1H-pyrrolo[2,3-b]pyridin-5-yl)phenyl)-2,4-difluorobenzenesulfonamide (6s). Compound **6s** was prepared (36 mg, 45% yield) according to GP I from *N*-(3-amino-5-(4,4,5,5-tetramethyl-1,3,2-dioxaborolan-2-yl)phenyl)-2,4-difluorobenzenesulfonamide (104 mg, 0.254 mmol) and 5-bromo-3-(pyridin-4-yl)-1H-pyrrolo[2,3-b]pyridine (46 mg, 0.17 mmol). ^1H NMR (300 MHz, CD_3OD) δ 6.57 (t, $J = 1.9$ Hz, 1H), 6.71 (d, $J = 1.7$ Hz, 1H), 6.73 (d, $J = 1.7$ Hz, 1H), 7.04–7.18 (m, 2H), 7.78 (d, $J = 6.3$ Hz, 2H), 7.90–7.98 (m, 1H), 8.02 (s, 1H), 8.38 (d, $J = 1.9$ Hz, 1H), 8.39 (s, 1H), 8.53 (d, $J = 6.2$ Hz, 2H). ^{13}C NMR (100 MHz, DMSO- d_6) δ 103.9, 105.8, 106.0, 106.2, 106.3, 109.0, 111.6, 112.1, 112.2, 112.4, 112.4, 116.9, 120.4, 124.0, 124.0, 124.1, 124.2, 125.2, 127.3, 129.8, 132.5, 132.6, 138.2, 140.0, 142.0, 142.3, 148.8, 149.9, 150.0. HRMS (EI+) m/z calcd for $\text{C}_{24}\text{H}_{17}\text{F}_2\text{N}_5\text{O}_2\text{S}$ [$\text{M} + \text{H}$] $^+$, 478.1149; found, 478.1120.

N-(3-Amino-5-(3-(pyridin-4-yl)-1H-pyrrolo[2,3-b]pyridin-5-yl)phenyl)-3-(trifluoromethyl)benzenesulfonamide (6t). Compound **6t** was prepared (37 mg, 49% yield) according to GP I from *N*-(3-amino-5-(4,4,5,5-tetramethyl-1,3,2-dioxaborolan-2-yl)phenyl)-3-(trifluoromethyl)benzenesulfonamide (98 mg, 0.22 mmol) and 5-bromo-3-(pyridin-4-yl)-1H-pyrrolo[2,3-b]pyridine (41 mg, 0.15 mmol). ^1H NMR (DMSO- d_6 , 300 MHz) δ 5.33 (s, 2H), 6.44 (s, 1H), 6.50 (s, 1H), 6.60 (s, 1H), 7.74 (d, $J = 6.1$ Hz, 2H), 7.80–7.85 (m, 1H), 8.00 (d, $J = 7.5$ Hz, 1H), 8.07–8.09 (m, 2H), 8.24 (d, $J = 2.6$ Hz, 1H), 8.28 (s, 1H), 8.29 (s, 1H), 8.55 (d, $J = 6.0$ Hz, 2H), 10.24 (s, 1H), 12.30 (s, 1H). ^{13}C NMR (100 MHz, DMSO- d_6) δ 104.6, 106.9, 109.3, 111.6, 116.9, 120.4, 123.3 (q, $J = 271$ Hz), 123.4, 125.1, 127.3, 129.5, 129.7, 129.8 (q, $J = 33$ Hz), 130.8, 130.9, 138.4, 140.1, 140.8, 141.9, 142.3, 148.8, 150.0, 150.1. HRMS (EI+) m/z calcd for $\text{C}_{25}\text{H}_{18}\text{F}_3\text{N}_5\text{O}_2\text{S}$ [$\text{M} + \text{H}$] $^+$, 510.1212; found, 510.1183.

N-(3-Amino-5-(3-(pyridin-4-yl)-1H-pyrrolo[2,3-b]pyridin-5-yl)-phenyl)acetamide (**6u**). Compound **6u** was prepared (30 mg, 48% yield) according to GP I from *N*-(3-amino-5-(4,4,5,5-tetramethyl-1,3,2-dioxaborolan-2-yl)phenyl)acetamide (65 mg, 0.24 mmol) and 5-bromo-3-(pyridin-4-yl)-1H-pyrrolo[2,3-b]pyridine (50 mg, 0.18 mmol). ¹H NMR (300 MHz, DMSO-*d*₆) δ 2.02 (s, 3H), 5.22 (s, 2H), 6.60 (s, 1H), 6.96 (s, 1H), 7.03 (s, 1H), 7.77 (d, *J* = 6.1 Hz, 2H), 8.24 (d, *J* = 2.6 Hz, 1H), 8.39 (s, 1H), 8.44 (d, *J* = 1.8 Hz, 1H), 8.56 (d, *J* = 6.1 Hz, 2H), 9.74 (s, 1H), 12.28 (s, 1H). ¹³C NMR (100 MHz, DMSO-*d*₆) δ 24.1, 103.6, 106.0, 107.9, 111.6, 116.9, 120.3, 125.1, 127.1, 130.3, 139.4, 140.5, 142.1, 142.4, 148.7, 149.5, 150.0, 168.1. HRMS (EI+) *m/z* calcd for C₂₀H₁₇N₅O [M + Na]⁺, 366.1331; found, 344.1328.

4-Methoxy-3-(3-(pyridin-4-yl)-1H-pyrrolo[2,3-b]pyridin-5-yl)-aniline (**6v**). Compound **6v** was prepared (5.5 mg, 15% yield) according to GP III from 3-bromo-4-methoxyaniline (27 mg, 0.12 mmol). ¹H NMR (300 MHz, CD₃OD) δ 2.91 (s, 3H), 5.97 (dd, *J* = 8.6, 2.8 Hz, 1H), 6.06 (d, *J* = 2.7 Hz, 1H), 6.12 (d, *J* = 8.6 Hz, 1H), 6.97 (dd, *J* = 4.7, 1.6 Hz, 2H), 7.20 (s, 1H), 7.59 (d, *J* = 1.9 Hz, 1H), 7.65 (d, *J* = 2.0 Hz, 1H), 7.70 (dd, *J* = 4.7, 1.6 Hz, 2H). HRMS (EI+) *m/z* calcd for C₁₉H₁₆N₄O [M + H]⁺, 317.1402; found, 317.1409.

N-(4-Amino-2-(3-(pyridin-4-yl)-1H-pyrrolo[2,3-b]pyridin-5-yl)-phenyl)benzenesulfonamide (**6w**). Compound **6w** was prepared (8 mg, 22% yield) according to GP III from *N*-(4-amino-2-bromophenyl)benzenesulfonamide (27 mg, 0.08 mmol). ¹H NMR (300 MHz, CD₃OD) δ 6.61–6.75 (m, 2H), 6.96 (d, *J* = 8.5 Hz, 1H), 7.12 (t, *J* = 7.5 Hz, 2H), 7.21–7.27 (m, 1H), 7.30–7.42 (m, 2H), 7.75–7.84 (m, 2H), 8.05 (s, 1H), 8.11 (s, 2H), 8.54 (d, *J* = 5.5 Hz, 2H). HRMS (EI+) *m/z* calcd for C₂₄H₁₉N₅O₂S [M + H]⁺, 442.1338; found, 442.1320.

Homology Modeling of TrkA. Because the 3D structure of TrkA has not been reported so far, we carried out homology modeling using the X-ray crystal structure of insulin-like growth factor 1 receptor (IGF1R, PDB entry 3I81)²² as the template to obtain a high-quality structure of TrkA suitable docking simulations. Sequence alignment between the kinase domains of TrkA and IGF1R was derived with the ClustalW program using the BLOSUM matrices for scoring the alignments. The parameters of GAP OPEN, GAP EXTENSION, and GAP DISTANCE were set equal to 10, 0.05, 8, respectively. Opening and extension gap penalties were thus changed systematically, and the obtained alignment was inspected for violation of structural integrity in the structurally conserved regions. On the basis of the best-scored sequence alignment, the 3D structure of the catalytic domain of TrkA was constructed using the latest version of the MODELLER program. In this model building, we employed an optimization method involving conjugate gradients and molecular dynamics to minimize the violations of the spatial restraints. With respect to the structure of gap regions, the coordinates were built from a randomized distorted structure that resides approximately between the two anchoring regions as implemented in the MODELLER program. To increase the accuracy of the calculated structures, loop modeling was also performed with the enumeration algorithm. Then we calculated the conformational energies of the predicted structures of TrkA with the ProSa 2003 program² for the purpose of evaluation.

Docking. We used the AutoDock program because the out-performance of its scoring function over those of the others had been shown in several target proteins. The atomic coordinates of TrkA obtained from the homology modeling were used as the receptor model with docking simulations. Special attention was paid to assign the protonation states of the ionizable Asp, Glu, His, and Lys residues in the homology-modeled structure of TrkA. The side chains of Asp and Glu residues were assumed to be neutral if one of their carboxylate oxygens pointed toward a hydrogen-bond-accepting group including the backbone aminocarbonyl oxygen at a distance within 3.5 Å, a generally accepted distance limit for a hydrogen bond of moderate strength. Similarly, the lysine side chains were protonated unless the NZ atom was in proximity to a hydrogen-bond donating group. The same procedure was also applied to determine the protonation states of ND and NE atoms in His residues. After determining the protonation state of each protein atom, we carried out 200 cycles of

energy minimization with the AMBER program to remove the bad steric contacts in the structure of TrkA.

Biological Assays and Methods. *Trk Enzyme Assay.* The IC₅₀ determinations were performed using radiometric kinase assays ([^γ-³³P]ATP) at the Reaction Biology Corp. (Malvern, PA, U.S.). Compounds were tested in a 10-dose IC₅₀ mode with 3-fold serial dilution starting at 1 μM. POC and K_d determinations were performed at the Ambit Bioscience Corp (San Diego, CA, U.S.). Compounds were profiled at 1 μM against a panel of 96 kinases in a high-throughput binding assay (Ambit Bioscience).

Cells and Materials. The human breast cell lines MDA-MB-231, MCF-7, and SKBR3 breast cancer cells were purchased from ATCC (Manassas, VA). FBS, medium, penicillin–streptomycin, and all other agents used in cell culture studies were purchased from Invitrogen (Carlsbad, CA). Cultures were maintained at 37 °C in a CO₂ incubator with a controlled humidified atmosphere composed of 95% air and 5% CO₂. HUVECs were grown in a gelatin coated 75 cm² flask in an M199 medium containing 3 ng/mL basic fibroblast growth factor (bFGF), 5 U/mL heparin, and 20% FBS at 37 °C in a humidified atmosphere of 5% CO₂/95% air.

Cell Growth/Proliferation. Cell viability was performed by MTT. Briefly, MDA-MB-231, MCF-7, and SKBR3 breast cancer cells were plated at a density of (5–10) × 10³ cells/well in 96-well plates for 24 h. Then the medium was removed, and cells were treated with either DMSO as a control or various concentrations of **6t**. The final concentration of DMSO in the medium was ≤0.1% (v/v). After the cells were incubated for 48 h, supernatants were removed from the wells and 10 μL MTT solutions (2 mg/mL) were added to each well for another 4 h at 37 °C. The formazan crystals that formed were dissolved in DMSO (100 μL/well) by constant shaking for 5 min. The plate was then read on a microplate reader at 540 nm. Six replicate wells were used for each analysis.

DAPI Staining and TUNEL Assay. MCF-7 cells were plated onto an 18 mm cover glass in RPMI-1640 medium at ~70% confluence for 24 h. The cells were then treated with **6t** at 10 μM for 24 h. They were fixed in ice-cold 2% paraformaldehyde (PFA), washed with PBS, and then stained with 2 μg/mL 4,6-diamidino-2-phenylindole (DAPI) for 20 min at 37 °C. The stained cells were examined under a fluorescence of nuclear fragmentation. Terminal deoxynucleotidyl transferase-mediated nick end labeling (TUNEL) was performed following the manufacturer's protocol for TUNEL kit (Chemicon, Temecula, CA).

Wound Migration Assay. HUVECs plated on 60 mm diameter culture dishes at 90% confluence were wounded with a razor blade score 2 mm in width and marked at the injury line. After wounding, the peeled off cells were removed with a serum-free medium and further incubated in M199 with 2% FBS, 1 mM thymidine (Sigma-Aldrich), and **6t** (1–10 μM). HUVECs were allowed to migrate for 16 h and were rinsed with a serum-free medium, followed by fixing with absolute alcohol.

Tube Formation Assay. Matrigel (200 μL) (10 mg/mL) (BD Biosciences, NJ) was polymerized for 30 min at 37 °C. HUVECs were suspended in M199 (5% FBS) medium at a density of 1.0 × 10⁵ cells/mL, and 0.2 mL of cell suspension was added to each well coated with Matrigel, together with or without the indicated concentrations of **6t** for 10 h. The morphological changes of the cells and HUVEC tubes formation were observed under a phase-contrast microscope and photographed at ×200 magnification.

■ ASSOCIATED CONTENT

📄 Supporting Information

Effect of **6t** on apoptosis of cancer cells. This material is available free of charge via the Internet at <http://pubs.acs.org>.

■ AUTHOR INFORMATION

Corresponding Author

*For S.-S.H.: phone, (+82) 32-890-3683; fax, (+82) 32-890-2462; e-mail, hongsg@inha.ac.kr. For S.H.: phone, (+82) 42-350-2811; fax, (+82) 42-350-2810; e-mail, hongorg@kaist.ac.kr.

Author Contributions

[§]These authors contributed equally to this work.

Notes

The authors declare no competing financial interest.

ACKNOWLEDGMENTS

This research was supported by National Research Foundation of Korea (NRF) through General Research Grants NRF-2011-0016436 and 2011-0020322. S.H. is the recipient of a Global Ph.D. Fellowship (Grant NRF-2011-0007581).

ABBREVIATIONS USED

RTK, receptor tyrosine kinase; TrkA, tropomyosin-related kinase A; HIF-1, hypoxia-inducible factor; VEGF, vascular endothelial growth factor; PI3K, phosphoinositide 3-kinase; iNOS, inducible nitric oxide synthase; HUVEC, human umbilical vein endothelial cell; ATP, adenosine 5'-triphosphate; SAR, structure-activity relationship; NIC, *N*-iodosuccinimide; DCM, dichloromethane; DMF, *N,N*-dimethylformamide; DIPE, diisopropyl ether; DPPE, 1,1'-bis(diphenylphosphino)-ferrocene; NBS, *N*-bromosuccinimide; MTT, 3-(4,5-dimethylthiazol-2-yl)-2,5-diphenyltetrazolium bromide

REFERENCES

- (1) Wang, T.; Yu, D.; Lamb, M. L. Trk kinase inhibitors as new treatments for cancer and pain. *Expert Opin. Ther. Pat.* **2009**, *19*, 305–319.
- (2) Patapoutian, A.; Reichardt, L. F. Trk receptors: mediators of neurotrophin action. *Curr. Opin. Neurobiol.* **2001**, *11*, 272–280.
- (3) Nakagawara, A. Trk receptor tyrosine kinases: a bridge between cancer and neural development. *Cancer Lett.* **2001**, *169*, 107–114.
- (4) Schramm, A.; Schulte, J. H.; Astrahantseff, K.; Apostolov, O.; Limpt, V.; Sieverts, H.; Kuhfittig-Kulle, S.; Pfeiffer, P.; Versteeg, R.; Eggert, A. Biological effects of TrkA and TrkB receptor signaling in neuroblastoma. *Cancer Lett.* **2005**, *228*, 143–153.
- (5) Adriaenssens, E.; Vanhecke, E.; Saule, P.; Mougel, A.; Page, A.; Romon, R.; Nurcombe, V.; Le Bourhis, X.; Hondermarck, H. Nerve growth factor is a potential therapeutic target in breast cancer. *Cancer Res.* **2008**, *68*, 346–351.
- (6) Weeraratna, A. T.; Dalrymple, S. L.; Lamb, J. C.; Denmeade, S. R.; Miknyoczki, S.; Dionne, C. A.; Isaacs, J. T. Pan-Trk inhibition decreases metastasis and enhances host survival in experimental models as a result of its selective induction of apoptosis of prostate cancer cells. *Clin. Cancer Res.* **2001**, *7*, 2237–2245.
- (7) Brodeur, G. M.; Minturn, J. E.; Ho, R.; Simpson, A. M.; Iyer, R.; Varela, C. R.; Light, J. E.; Kolla, V.; Evans, A. E. Trk receptor expression and inhibition in neuroblastomas. *Clin. Cancer Res.* **2009**, *15*, 3244–3250.
- (8) Lagadec, C.; Meignan, S.; Adriaenssens, E.; Foveau, B.; Vanhecke, E.; Romon, R.; Toillon, R. A.; Oxombre, B.; Hondermarck, H.; Le Bourhis, X. TrkA overexpression enhances growth and metastasis of breast cancer cells. *Oncogene* **2009**, *28*, 1960–1970.
- (9) Nakamura, K.; Tan, F.; Li, Z.; Thiele, C. J. NGF activation of TrkA induces vascular endothelial growth factor expression via induction of hypoxia-inducible factor-1 α . *Mol. Cell. Neurosci.* **2011**, *46*, 498–506.
- (10) Romon, R.; Adriaenssens, E.; Lagadec, C.; Germain, E.; Hondermarck, H.; Le Bourhis, X. Nerve growth factor promotes breast cancer angiogenesis by activating multiple pathways. *Mol. Cancer* **2011**, *9*, 157–169.
- (11) Wood, E. R.; Kuyper, L.; Petrov, K. G.; Hunter, R. N.; Harris, P. A.; Lackey, K. Discovery and in vitro evaluation of potent TrkA kinase inhibitors: oxindole and aza-oxindoles. *Bioorg. Med. Chem. Lett.* **2004**, *14*, 953–957.
- (12) Gingrich, D. E.; Yang, S. X.; Gessner, G. W.; Angeles, T. S.; Hudkins, R. L. Synthesis, modeling, and in vitro activity of (3'S)-epi-K-

252a analogues. Elucidating the stereochemical requirements of the 3'-sugar alcohol on TrkA tyrosine kinase activity. *J. Med. Chem.* **2005**, *48*, 3776–3783.

- (13) Lippa, B.; Morris, J.; Corbett, M.; Kwan, T. A.; Noe, M. C.; Snow, S. L.; Gant, T. G.; Mangiaracina, M.; Coffey, H. A.; Foster, B.; Knauth, E. A.; Wessel, M. D. Discovery of novel isothiazole inhibitors of the TrkA kinase: structure-activity relationship, computer modeling, optimization, and identification of highly potent antagonists. *Bioorg. Med. Chem. Lett.* **2006**, *16*, 3444–3448.

- (14) Wang, T.; Lamb, M. L.; Scott, D. A.; Wang, H.; Block, M. H.; Lyne, P. D.; Lee, J. W.; Davies, A. M.; Zhang, H. J.; Zhu, Y.; Gu, F.; Han, Y.; Wang, B.; Mohr, P. J.; Kaus, R. J.; Josey, J. A.; Hoffmann, E.; Thress, K.; Macintyre, T.; Wang, H.; Omer, C. A.; Yu, D. Identification of 4-aminopyrazolopyrimidines as potent inhibitors of Trk kinases. *J. Med. Chem.* **2008**, *51*, 4672–4684.

- (15) Kim, S.-H.; Tokarski, J. S.; Leavitt, K. J.; Fink, B. E.; Salvati, M. E.; Moquin, R.; Obermeier, M. T.; Trainor, G. L.; Vite, G. G.; Stadnick, L. K.; Lippy, J. S.; You, D.; Lorenzi, M. V.; Chen, P. Identification of 2-amino-5-(thioaryl)thiazoles as inhibitors of nerve growth factor receptor TrkA. *Bioorg. Med. Chem. Lett.* **2008**, *18*, 634–639.

- (16) Tripathy, R.; Angeles, T. S.; Yang, S. X.; Mallamo, J. P. TrkA kinase inhibitors from a library of modified and isosteric staurosporine aglycone. *Bioorg. Med. Chem. Lett.* **2008**, *18*, 3551–3555.

- (17) Mauro Mileni, M.; Garfinkle, J.; Ezzili, C.; Kimball, F. S.; Cravatt, B. F.; Stevens, R. C.; Boger, D. L. X-ray crystallographic analysis of α -ketoheterocycle inhibitors bound to a humanized variant of fatty acid amide hydrolase. *J. Med. Chem.* **2010**, *53*, 230–240.

- (18) Lee, K. M.; Choi, W. J.; Lee, Y.; Lee, H. J.; Zhao, L. X.; Lee, H. W.; Park, J. G.; Kim, H. O.; Hwang, K. Y.; Heo, Y.-S.; Choi, S.; Jeong, L. S. X-ray crystal structure and binding mode analysis of human S-adenosylhomocysteine hydrolase complexed with novel mechanism-based inhibitors, haloneplanocin A analogues. *J. Med. Chem.* **2011**, *54*, 930–938.

- (19) (a) Baek, D. J.; Seo, J.-H.; Lim, C.; Kim, J. H.; Chung, D. H.; Cho, W.-J.; Kang, C.-Y.; Kim, S. The 3-deoxy analogue of a-GalCer: disclosing the role of the 4-hydroxyl group for CD1d-mediated NKT cell activation. *ACS Med. Chem. Lett.* **2011**, *2*, 544–548. (b) Baek, D. J.; Lee, Y.-S.; Lim, C.; Lee, D.; Lee, T.; Lee, J.-Y.; Lee, K.-A.; Cho, W.-J.; Kang, C.-Y.; Kim, S. Rational design and evaluation of a branched chain-containing glycolipid antigen that binds to CD1d. *Chem.—Asian J.* **2010**, *5*, 1560–1564.

- (20) Hong, S.; Lee, S.; Kim, B.; Lee, H.; Hong, S.-S.; Hong, S. Discovery of new azaindole-based PI3K α inhibitors: apoptotic and antiangiogenic effect on cancer cells. *Bioorg. Med. Chem. Lett.* **2010**, *20*, 7212–7215.

- (21) (a) Morris, G. M.; Goodsell, D. S.; Halliday, R. S.; Huey, R.; Hart, W. E.; Belew, R. K.; Olson, A. J. Automated docking using a Lamarckian genetic algorithm and an empirical binding free energy function. *J. Comput. Chem.* **1998**, *19*, 1639–1662. (b) Park, H.; Chi, O.; Kim, J.; Hong, S. Identification of novel inhibitors of tropomyosin-related kinase A with structure-based virtual screening with homology modeled protein structure. *J. Chem. Inf. Model.* **2011**, *51*, 2986–2993.

- (22) Wittman, M. D.; Carboni, J. M.; Yang, Z.; Lee, F. Y.; Antman, M.; Attar, R.; Balimane, P.; Chang, C.; Chen, C.; Discenza, L.; Frennesson, D.; Gottardis, M. M.; Greer, A.; Hurlburt, W.; Johnson, W.; Langley, D. R.; Li, A.; Li, J.; Liu, P.; Mastalerz, H.; Mathur, A.; Menard, K.; Patel, K.; Sack, J.; Sang, X.; Saulnier, M.; Smith, D.; Stefanski, K.; Trainor, G.; Velaparthi, U.; Zhang, G.; Zimmermann, K.; Vyas, D. M. Discovery of a 2,4-disubstituted pyrrolo[1,2-*f*][1,2,4]-triazine inhibitor (BMS-754807) of insulin-like growth factor receptor (IGF-1R) kinase in clinical development. *J. Med. Chem.* **2009**, *52*, 7360–7363.

- (23) Sun, Q.; Wu, R.; Cai, S.; Lin, Y.; Sellers, L.; Sakamoto, K.; He, B.; Peterson, B. R. Synthesis and biological evaluation of analogues of AKT (protein kinase B) inhibitor-IV. *J. Med. Chem.* **2011**, *54*, 1126–1139.

- (24) Ashe, P. C.; Berry, M. D. Apoptotic signaling cascades. *Prog. Neuro-Psychopharmacol. Biol. Psychiatry* **2003**, *27*, 199–214.